

Selection and identification of an RNA aptamer that specifically binds the HIV-1 capsid lattice and inhibits viral replication

Paige R. Gruenke^{1,2,†}, Rachna Aneja^{3,†}, Sarah Welbourn⁴, Obiaara B. Ukah³, Stefan G. Sarafianos⁵, Donald H. Burke^{1,2,3} and Margaret J. Lange^{3,*}

¹Department of Biochemistry, University of Missouri, Columbia, MO 65211, USA, ²Bond Life Sciences Center, University of Missouri, Columbia, MO 65211, USA, ³Department of Molecular Microbiology & Immunology, School of Medicine, University of Missouri, Columbia, MO 65211, USA, ⁴Emory Vaccine Center and Yerkes National Primate Research Center, Emory University, Atlanta, GA 30329, USA and ⁵Laboratory of Biochemical Pharmacology, Department of Pediatrics, Emory University School of Medicine, Atlanta, GA 30322, USA

Received September 20, 2021; Revised November 23, 2021; Editorial Decision December 13, 2021; Accepted December 16, 2021

ABSTRACT

The HIV-1 capsid core participates in several replication processes. The mature capsid core is a lattice composed of capsid (CA) monomers thought to assemble first into CA dimers, then into ~250 CA hexamers and 12 CA pentamers. CA assembly requires conformational flexibility of each unit, resulting in the presence of unique, solvent-accessible surfaces. Significant advances have improved our understanding of the roles of the capsid core in replication; however, the contributions of individual CA assembly forms remain unclear and there are limited tools available to evaluate these forms *in vivo*. Here, we have selected aptamers that bind CA lattice tubes. We describe aptamer CA15-2, which selectively binds CA lattice, but not CA monomer or CA hexamer, suggesting that it targets an interface present and accessible only on CA lattice. CA15-2 does not compete with PF74 for binding, indicating that it likely binds a non-overlapping site. Furthermore, CA15-2 inhibits HIV-1 replication when expressed in virus producer cells, but not target cells, suggesting that it binds a biologically-relevant site during virus production that is either not accessible during post-entry replication steps or is accessible but unaltered by aptamer binding. Importantly, CA15-2 represents the first aptamer that specifically recognizes the HIV-1 CA lattice.

INTRODUCTION

The HIV-1 capsid (CA) protein plays an indispensable role in both early and late stages of viral replication, performing multifaceted functions that extend beyond housing the viral RNA and proteins required for replication (1–8). The capsid core facilitates reverse transcription and formation of the pre-integration complex (2,3,9–11), enables transport through the cytosol to the nucleus via interactions with a variety of host factors (3,12–15), facilitates nuclear import (1,3,8,16–20), delivers the pre-integration complex for integration into the host chromosome (18–25), and enables HIV-1 to evade host innate immune surveillance during replication (6,26–28). CA also plays a significant role in viral assembly and maturation (8,11,29,30). As disruption of any of these events can significantly impact viral replication, the viral capsid core is an important target both for better understanding virus biology and developing new therapeutics to combat the ongoing AIDS pandemic.

Prior work has highlighted the dynamic nature of the viral capsid core. The mature capsid lattice is composed of ~1500 CA monomers thought to assemble first into CA dimers, then into ~250 CA hexamers and 12 pentamers that facilitate the curvature of the mature capsid core (31). Each CA monomer contains independently folded N-terminal (CA_{NTD}) and C-terminal (CA_{CTD}) domains that are connected by a flexible linker (32–35). Neighboring subunits in each hexamer and pentamer are connected by intermolecular CA_{NTD}–CA_{NTD} and CA_{NTD}–CA_{CTD} interactions, while pairs of subunits between hexamers are connected by dimeric and trimeric CA_{CTD}–CA_{CTD} contacts (33–39). Interactions between the CA_{NTD} and CA_{CTD} regulate and stabilize the lattice in conjunction with a hydration

*To whom correspondence should be addressed. Tel: +1 573 882 0680; Email: langemj@missouri.edu

†The authors wish it to be known that, in their opinion, the first two authors should be regarded as Joint First Authors.

Present address: Margaret Lange, Department of Molecular Microbiology & Immunology, 471i Life Sciences Center, University of Missouri, Columbia, MO 65211, USA.

layer composed of thousands of water molecules (40,41). Assembly of CA into these independent states requires conformational flexibility of each CA protein (38,40), supporting the presence of unique, solvent-accessible binding surfaces on each assembly state. Replication events and thus viral infectivity can be severely compromised by mutations that impact lattice stability, alter interactions between or among CA assembly states, or disrupt the hydration layer (1,5,31,36,40,42–50). While destabilization must eventually occur for successful replication, a delicate balance between stability and dissociation must be maintained, demonstrating an intricate link between the capsid core and viral infectivity (3,5,6,9,46,51).

Substantial developments in protein engineering, structural biology, and molecular modeling have led to an improved understanding of the molecular architecture and interaction surfaces of various CA assembly forms (12,38,40,52–56). Indeed, several critical binding interactions between CA and host factors have been defined. These host factors include restriction factors such as TRIM5 α , TRIMCyp and MxB (27,57–67), and infectivity factors such as Cyclophilin A (CypA), cleavage and polyadenylation specific factor 6 (CPSF6), nucleoporin 153 (Nup153), and recently identified Sec24C (11,15,68–73). Interestingly, several of these host factors share overlapping binding sites at CA hexamer junctions that are lost upon capsid core disassembly, illustrating the importance of assembly state-specific interactions (74). Small molecules also bind sites associated with specific assembly forms. The recent discovery of the stabilizing role of inositol hexakisphosphate (IP6) (75–80) has facilitated important developments such as the recent demonstration of efficient reverse transcription and integration by capsid cores in a cell-free system (2). The identification of small molecules that bind CA has also contributed to our understanding of the role of CA in HIV-1 replication. PF-3450074 (PF74), which binds to a pocket found at the CA_{NTD}–CA_{CTD} interface of assembled CA hexamers, has been shown to alter the stability of the CA lattice (71,81,82). PF74 seems to interfere with the interaction of the capsid core and host proteins, namely CPSF6 and NUP153 (69,71,74,82,83). Gilead compounds, GS-CA1 and GS-6207, more recently described CA-targeting small molecules that bind in the same pocket as PF74, interfere with both nuclear import of viral DNA and CA assembly (14,82,84). GS-6207 is currently in clinical trials. Importantly, the ability of known restriction factors and small molecules to specifically recognize different CA assembly forms supports the presence of unique, biologically relevant binding sites present on these CA assembly forms and underscores the importance of identifying novel targetable sites.

Despite these advances, there are many unresolved questions regarding CA structural dynamics and their impact on viral biology. Recent work supports the presence of partial Gag hexamers at the edges of the immature Gag hexamer lattice, which could serve as substrates for proteolytic maturation and contribute to assembly of the immature lattice (53). However, further study is required to fully understand the order in which immature lattice assembly occurs and how it leads to activation of the viral protease, as well as the assembly mechanisms underlying remodeling of pro-

teolytically cleaved CA into the mature capsid core. In addition, the mature capsid core may also undergo some degree of remodeling to facilitate reverse transcription, nuclear entry and integration (2). Indeed, dissociation is required for access of the proviral DNA to the host chromosome during integration, although the degree of dissociation required and the location at which dissociation begins remain controversial (18,19,21–25,51,85–88). Furthermore, we still do not fully understand the broad spectrum of CA interactions with host proteins and their implications for virus replication, and previously undescribed interactions and targetable surfaces likely exist. New tools are needed to support studies of the contributions of CA assembly forms to diverse replication events, to identify novel interaction sites on different CA assembly forms, or to compete with various host factors for binding to CA assembly forms.

To address these gaps, we sought to develop aptamers that specifically target accessible binding sites present on the assembled CA lattice. Aptamers are structured oligonucleotides generated through an enrichment process termed SELEX (Systematic Evolution of Ligands by EXponential enrichment) to bind molecular targets. Through adoption of highly structured 3D conformations, aptamers have been shown to discriminate among very similar proteins (e.g. a single amino acid change (89–91) or different conformations of the same protein (92–97)). Prior work has identified aptamers targeted to various HIV-1 proteins, including nucleocapsid (98), Gag polyprotein (99,100), integrase (101), reverse transcriptase (89,102–105), and others (106–108). Aptamers targeting the Gag polyprotein were demonstrated to bind the Gag polyprotein as well as the matrix (MA) or nucleocapsid (NC) components of Gag, likely due to the presence of highly basic regions in these proteins. Notably, some of the Gag aptamers were able to bind Gag and the CANC portion of Gag, but not NC alone. However, they were not reported to bind recombinant CA alone (99, 100) and failed to bind the assembled CA lattice utilized here (Supplemental Figure S1A). Thus, aptamers that specifically target HIV-1 CA or its assembly forms have not been previously described. In this study, we report the identification and characterization of aptamer CA15-2, which binds specifically the HIV-1 CA lattice, but not the CA monomer or CA hexamer. Binding was not dependent upon mutations introduced into the CA lattice construct, as CA15-2 was also able to bind assembled native CA lattice tubes. We also demonstrate that aptamer CA15-2 significantly inhibits HIV-1 replication in producer cells, but not in target cells.

MATERIALS AND METHODS

Reagents

Unless otherwise noted, all chemicals were purchased from Sigma-Aldrich (St. Louis, MO). The 56N library for aptamer selection, DNA templates for aptamer truncations and all primers were ordered from Integrated DNA Technologies (Coralville, IA).

Plasmid constructs for expression and purification of soluble HIV-1 CA hexamer (pET11a-CA (A14C, E45C, W184A and M185A)), CA hexamer lattice (pET11a-CA (A14C and E45C)), and CA monomer (pET11a-CA) were kindly provided by Dr Owen Pornillos and Dr Barbie

Ganser-Pornillos at the University of Virginia. For the purposes of the work described here, the CA hexamer lattice will be referred to as the CA lattice to avoid confusion with the soluble CA hexamer. The CMV-driven plasmid encoding aptamer or control RNA sequences flanked by stabilizing structures for expression in mammalian cells was developed previously (109). To insert anti-HIV-1 CA aptamers or controls into the expression plasmid, the aptamer expression plasmid was digested using *EcoRI* and *ApaI* (New England Biolabs, Ipswich, MA) and purified using agarose gel extraction. DNA encoding aptamers or control RNAs was amplified by PCR using appropriate primers to enable InFusion Cloning into Stellar competent cells (Takara Bio USA, Inc., Mountain View, CA). Sequences of aptamers, control RNAs and amplification primers are listed in Table 1. All plasmids were confirmed by DNA sequencing. The HIV-1_{NL3-4}-derived CMV-EGFP plasmid (pNL4-3-CMV-EGFP) used in single-cycle infectivity assays was kindly provided by Vineet KewalRamani (National Cancer Institute [NCI]-Fredrick) and has been previously described (109). The vesicular stomatitis virus glycoprotein (VSV-G)-expressing plasmid, pMD-G, was obtained from Invitrogen (Carlsbad, CA).

Biological resources

The human cell lines 293FT (Invitrogen, Carlsbad, CA) and TZM-GFP (110) were maintained in standard culture media containing Dulbecco's Minimum Essential Medium (Sigma, St. Louis, MO), 10% FBS (Sigma, St. Louis, MO), 2 mM L-glutamine (Gibco, Life Technologies, Grand Island, NY), 1 mM non-essential amino acids (Gibco, Life Technologies, Grand Island, NY), and 1 mM sodium pyruvate (Gibco, Life Technologies, Grand Island, NY). The 293FT cells were cultured in 0.5 mg/mL G418 (Sigma, St. Louis, MO). All cell lines were maintained at 37°C in 5% carbon dioxide with splitting approximately three times per week.

Expression and purification of HIV-1 CA proteins and crosslinking of CA hexamers and CA lattice tubes

Purified, assembled HIV-1 CA lattice for the aptamer selection was kindly provided by Dr Owen Pornillos and Dr Barbie Ganser-Pornillos at the University of Virginia. Post-selection experiments were performed using newly purified proteins, which were expressed and purified as previously described (37,111). Briefly, the HIV-1 CA proteins were expressed by IPTG induction in *Escherichia coli* BL21(DE3) cells for 6–12 h at 25°C. The monomeric p24 CA protein was purified using a Hi-Trap Q-Sepharose column after ammonium sulfate precipitation. Homogenously purified protein fractions were concentrated and reconstituted in 25 mM Tris–HCl (pH 8.1) and 40 mM NaCl, flash frozen and stored at –80°C.

Soluble CA hexamers (pET11a-CA (A14C/E45C/W184A/M185A)) and CA lattice tubes (pET11a-CA (A14C/E45C)) were assembled as previously described (34,37). Briefly, assembly was performed *in vitro* by sequential overnight dialysis. Pooled and concentrated fractions were dialyzed into assembly buffer (50 mM Tris, pH 8.1, 1 M NaCl, and 200 mM βME) followed

by dialysis into storage buffer (20 mM Tris, pH 8.1, and 40 mM NaCl). The integrity of the assembled CA lattice tubes was verified using transmission electron microscopy (TEM) with assistance from the University of Missouri Electron Microscopy Core (Supplemental Figure S1B). Diluted CA lattice was spotted onto grids and stained with uranyl acetate (34,37). Tubes were visualized on the JEOL JEM-1400 120 kV TEM. The purity and integrity of monomeric p24, assembled soluble CA hexamers and CA lattice were confirmed by non-reducing SDS-PAGE (Supplemental Figure S1C). Importantly, for the purposes of this study, all CA protein concentrations are reported in terms of the total CA monomer.

Assembly of native capsid tubes

To determine the ability of compound 15 (112,113) to facilitate assembly of native CA at physiological salt concentrations, assembly of 200 μM native CA monomer into assembled native CA lattice tubes was initiated in 1× binding buffer by adding compound 15 to a final concentration of 20 μM from a 100 μM stock containing 10% DMSO. Absorbance at 350 nm was monitored at 1 min intervals using a BioTek Synergy HT plate reader (BioTek Instruments, Winooski, VT) for 120 min. In addition, the absorbance at 350 nm for negative control samples containing only the capsid protein or the capsid protein and DMSO were also monitored.

To prepare native CA lattice tubes for nitrocellulose filter binding assays, 100 μM working stocks of compound 15 were prepared using a final concentration of 10% DMSO. Native CA lattice tubes were assembled by incubating 200 μM CA monomer and 20 μM compound 15 in 1× binding buffer at 37°C for 1 h. Assembled tubes were pelleted by centrifugation at 16000 × g for 5 min. The supernatant was removed, and the pelleted tubes were washed with 1× binding buffer containing 20 μM compound 15. The centrifugation step was repeated, and the supernatant was removed. The native capsid tubes were resuspended in 1× binding buffer containing 20 μM compound 15 for subsequent binding assays.

CA lattice aptamer selection

Prior to the first round of selection, the double-stranded 56N library transcription template was generated from the bottom strand of the 56N starting library in a 10 ml PCR. The top strand of the 56N starting library transcription template and all relevant primers are listed in Table 1. The total transcript length is 104 nucleotides. The selection was initiated using ~10¹⁵ unique sequences in a 1 ml transcription.

Run-off transcription reactions were performed using the Y639F mutant T7 RNA polymerase (114), *in vitro* transcription buffer (50 mM Tris–HCl pH 7.5, 15 mM MgCl₂, 5 mM DTT and 2 mM spermidine), and 2 mM each NTP. Reactions were incubated at 37°C for a minimum of 4 h and halted by adding an equal volume of denaturing gel loading buffer (90% formamide and 50 mM EDTA with trace amounts of xylene cyanol and bromophenol blue). RNAs were purified by denaturing polyacrylamide gel elec-

Table 1. Aptamer and primer sequences used in this study^a

Name	Sequence
56N Library Top Strand ^b	GCCTAATACGACTCACTATAGGAAGAAGAGAATCATACACAAGA-(N) ₅₆ -GGGCA TAAGGTAGGTAAGTCCATA
56N Forward Primer	GCCTAATACGACTCACTATAGGAAGAAGAGAATCATACACAAGA
56N Reverse Primer	TATGGACTTACCTACCTTATGCCC
56N InFusion Forward Primer	CCTTGTATCTGAATTCCAAGAGAATCATACACAAGA
56N InFusion Reverse Primer	CACAATCCGTGACAGGGCCCTATGGACTTACCTACCTTATGCCC
Arb Forward Primer	GCCTAATACGACTCACTATAGGGAAAAGCGAATCATACACAAGA
Arb Reverse Primer	TATGGAATTAATACCTTATGCCC
56N 5' Anti-Leader	TCTTGTGTATGATTCTTCTTCC
CA15-2	ggaagaagagaaucacacaagaUCGACGUACCUCAGGGUGGUGUAUGACUGAGGUGAA GACUGUGAACCAUGGCAUGCgggcauaagguagguaguccaua
CA8-4	ggaagaagagaaucacacaagaCCAGCGCGGUCCAGUAACAGCCGGCCCAUGCCGCC UACUGUCUUGCAGAUUCCACgggcauaagguagguaguccaua
CA8-6	ggaagaagagaaucacacaagaACAAGUGAUUAAGGAAGGUGUAUAGGAGGCGAAUC ACUGUAAGGUGUUGGAAUAgggcauaagguagguaguccaua
CA10-2	ggaagaagagaaucacacaagaCCAUCCCCAACUUGUCAAGAGGGAAGGAGUGGGAA AGGAAGACAAGGACAUGUGgggcauaagguagguaguccaua
CA10-5	ggaagaagagaaucacacaagaGGCGAAUACACGACAUCUGGACGACCUACACUAU GAGAGGAGGUGAGAGUGGAAAgggcauaagguagguaguccaua
CA15-1	ggaagaagagaaucacacaagaCCUACCUGUAUGAAAGAGACGAACCUAACUACAAUG CUAGCAAUGGUGUAUGGUGCgggcauaagguagguaguccaua
CA15-8	ggaagaagagaaucacacaagaCCGUGCCCAGGGUCUUGCUGUAUGUAUGGUGCUGAU CUACUGUAGCCAUGUGUAUGgggcauaagguagguaguccaua
Scrambled CA15-2	ggaagaagagaaucacacaagaGGAGGUGCAGGUGCAUAAUGCGUGAAGGCUCGGCCU GUACACUCGAAGUACUAGUgggcauaagguagguaguccaua
Arbitrary RNA	gggaaaagcgaucacacaagaAAUUUGGACUUUCCGCCUUUUGCCUUUAUGAGG AUCUCUCUGAUUUUUCUUGCGUCGAGUUUCCCGgggcauaagguauuuuuuuccaua
CA15-2 1-80 Stem Disrupt (1-80*)	ggaagaagagaaucacacaagaUCGACGUAGAGCAGGGUGGUGUAUGACUGAGGUGAA GACUGUGAACCAUGGCAUGC
CA15-2 1-80 Stem Rescue (1-80**)	ggaagaagagaaucacacaagaUCGACGUAGAGCAGGGUGGUGUAUGACUGCUCUGAA GACUGUGAACCAUGGCAUGC
CA15-2 25-104 ^c	GGUCGACGUACCUCAGGGUGGUGUAUGACUGAGGUGAAGACUGUGAACCA UGGCAUGCgggcauaagguagguaguccaua
CA15-2 25-80	GGUCGACGUAGAGCAGGGUGGUGUAUGACUGCUCUGAAGACUGUGAACCA UGGCAUGC
CA15-2 25-60	GGUCGACGUAGAGCAGGGUGGUGUAUGACUGCUCUGAA
CA15-2 30-60	GUACCUCAGGGUGGUGUAUGACUGAGGUGAA

^aThe constant regions for the RNAs are in lowercase. ^bThe T7 promoter is underlined. ^cFor CA15-2 transcripts beginning at position 25, two guanine nucleotides (underlined) were added to the 5' end to aid in *in vitro* transcription. The addition of these nucleotides did not alter the predicted secondary structures represented in Figure S6.

trophoresis (6% TBE-PAGE, 8 M urea). Bands corresponding to the expected product sizes were visualized by UV shadow, excised, and eluted overnight in 300 mM sodium acetate (pH 5.4) at room temperature. Eluates were ethanol precipitated, resuspended in nuclease-free water and stored at -20°C until further use. RNA concentrations were determined using a NanoDropOne spectrophotometer (Thermo Fisher Scientific, Waltham, MA). For the first round of selection, 5 nmol of RNA (~3.0 × 10¹⁵ molecules) was used, followed by 1.5 nmol RNA (~9.0 × 10¹⁴ molecules) in subsequent rounds. Prior to each selection round, the RNA was refolded by heating to 90°C for 90 s followed by cooling to room temperature for 5 min. CA lattice solution was then added, followed by addition of 10X binding buffer to a final concentration of 1 × (50 mM Tris-HCl [pH 7.5], 100 mM KCl, 50 mM NaCl, 1 mM MgCl₂). For the first round of selection, 1 nmol CA lattice was added to the refolded RNA libraries in a final volume of 2 ml (2500 nM RNA to 500 nM lattice). In subsequent rounds, 300 pmol CA lattice was added in a final volume of 1 ml (1500 nM RNA to 300 nM lattice). Binding reactions were incubated at 37°C

for 15 min followed by partitioning of the bound versus unbound RNA species from the CA lattice by centrifugation at 16 000 × g for 10 min at 4°C. Following centrifugation, the supernatant containing unbound RNA species was removed and the CA lattice pellet was washed with 1X binding buffer. The sample was then centrifuged again at 16 000 × g for 10 min at 4°C. The wash step was performed a total of two times. CA lattice-bound RNA was recovered using phenol/chloroform extraction and ethanol precipitation. The recovered RNA was reverse transcribed using ImProm-II Reverse Transcriptase (Promega, Madison, WI) and PCR amplified using Pfu DNA polymerase to generate the transcription template for the next round of selection.

Library cloning into the aptamer expression plasmid

The double-stranded DNA templates for round 8, 10 and 15 libraries were cloned into an aptamer expression cassette as described above (see Plasmids). The resulting plasmids were purified from overnight cultures grown from single colonies picked from ampicillin-containing agar plates. Sanger se-

quencing was performed at the University of Missouri Genomics Technology Core to determine individual aptamer sequences for each clone. Aptamers were named according to the round and clone number. For example, aptamer 15-2 was the sequence present in the second colony picked from the round 15 plate.

DNA templates and RNA transcription

RNA aptamers (Table 1) were generated each clone described above for use in biochemical assays. Transcription templates were generated by PCR amplification of the aptamer expressing plasmids described above using Pfu DNA polymerase, the 56N forward primer to append the T7 promoter, and the reverse primer complementary to the 3' constant region. Amplicon size was confirmed by agarose gel electrophoresis. Amplicons were transcribed *in vitro* and purified as described above.

Nitrocellulose filter binding assays

In vitro transcribed RNA was treated with Antarctic phosphatase (Fermentas, Waltham, MA) to remove the 5' terminal phosphate and then labeled by T4 polynucleotide kinase (New England Biolabs, Ipswich, MA) in the presence of γ -³²P-labeled ATP (PerkinElmer, Waltham, MA). Radiolabeled RNAs were gel-purified using denaturing PAGE as described above. To evaluate dose-dependent binding of aptamer libraries or individual aptamers to CA proteins, 50 nM 5'-radiolabeled and refolded RNA was incubated with varying concentrations of CA lattice, CA hexamer, or CA monomer in 1× binding buffer at 37°C for 15 min. A separate aliquot of the same RNA was incubated with 0 nM CA protein to determine non-specific nucleic acid retention. RNA:protein complexes were partitioned from unbound RNA by filtering samples through a pre-wet, alkaline-treated nitrocellulose filter under vacuum and immediately washing with 1 mL binding buffer. Radioactivity retained on the filter was counted by placing filters into scintillation vials, adding 4 ml Emulsifier-safe liquid scintillation fluid (Perkin Elmer, Waltham, MA), and counting using a liquid scintillation counter. An unfiltered 'No Wash' sample was counted to determine the total amount of radioactivity present in each binding reaction. The fraction of RNA retained on the filter was calculated by dividing the radioactivity retained on the filter by the radioactivity present in the 'No Wash' sample. At least three replicates were performed for each binding assay. To decrease non-specific nucleic acid retention, nitrocellulose filters were pre-incubated in 0.5 M KOH for 20 min, washed extensively with MilliQ water, and then incubated in 1× binding buffer for at least 45 min as previously described (115).

To determine the apparent dissociation constant (K_{Dapp}) using nitrocellulose filter binding assays, ~20 000 counts-per-minute (cpm) of 5'-radiolabeled and refolded RNA was incubated with varying concentrations of CA lattice (0 nM CA lattice to determine non-specific binding, or 10 to 7500 nM CA lattice) in 1× binding buffer at 37°C for 15 min. The nitrocellulose filter binding assay was then performed as described above. The values for the fraction of RNA retained on filter were fit to a 1:1 binding curve model

($Y = B_{max} * X / [K_D + X]$) using GraphPad Prism 6.2. In the equation, B_{max} is the maximum specific binding, K_D is the dissociation constant, X is the CA concentration (total monomer), and Y is the fraction of RNA retained on filter. Binding assays were performed in triplicate.

To determine whether aptamer CA15-2 retained binding to CA lattice when an antisense oligonucleotide was annealed to either its 5' or 3' constant region, 50 nM 5'-radiolabeled CA15-2 RNA and 62.5 nM antisense oligonucleotide were mixed on ice in 1× binding buffer. For thermal renaturation and annealing of the antisense oligonucleotide to the aptamer, the samples were transferred into a preheated aluminum insert within a dry heat block set to 90°C for 1 min, then the aluminum insert was removed from the heat block and placed on the benchtop and allowed to cool to 37°C. 2 μM CA lattice (or 0 nM CA lattice to determine non-specific binding) was then added to each reaction, and the reaction was incubated at 37°C for 15 min. The nitrocellulose filter binding assay was then performed as described above to determine fraction RNA retained on filter. Experiments were performed at least three times.

To evaluate the effect of IP6 on CA15-2 binding to CA lattice, 50 nM 5'-radiolabeled and refolded CA15-2 or arbitrary RNA was incubated with 1 μM CA lattice at varying concentrations of IP6 (0 to 200 nM IP6) in 1× binding buffer at 37°C for 15 min. The nitrocellulose filter binding assay was then performed as described above to determine the fraction RNA retained on filter. These experiments were performed in triplicate.

To evaluate the effect of high salt concentration on CA15-2 binding to CA lattice, 50 nM 5'-radiolabeled and refolded CA15-2 or arbitrary RNA was incubated in varying concentration of assembled CA lattice (0–1000 nM CA lattice) in high salt binding buffer (50 mM Tris-HCl [pH 7.5], 100 mM KCl, 1 M NaCl, 1 mM MgCl₂) at 37°C for 15 min. Nitrocellulose filter binding assays were performed as described above in triplicate.

To evaluate the ability of CA15-2 to bind assembled native CA lattice tubes, nitrocellulose filter binding assays were performed in the presence of 20 μM compound 15 for stabilization of the native CA lattice tubes.

Size exclusion chromatography for the complex of the CA lattice with aptamers

To determine whether CA15-2 forms stable complex with CA lattice, 100 nM refolded RNA (CA15-2 or Arbitrary) was combined with 1000 nM of CA lattice and incubated in 1× binding buffer for 30 min. Size exclusion chromatography (SEC) analysis was then performed using a Superdex 200 Increase 10/300GL column. RNA alone and CA lattice alone were also analyzed to define the peaks corresponding to the complex of RNA and the CA lattice. Experiments were performed in triplicate and representative curves of one experiment are shown in Figure S3A.

Dye conjugation to antisense oligos

The 56N reverse primer with a 5'-amino group attached to a C-6 alkyl chain (5' amino modifier C6) was purchased from Integrated DNA Technologies (Coralville, IA)

and used in a dye conjugation reaction with Cy5-NHS ester (Lumiprobe, Hunt Valley, MD). The conjugation reaction, subsequent reverse-phase HPLC purification, and concentration/buffer exchange of the Cy5-labeled 56N reverse primer were performed as described previously (116).

Electrophoretic mobility shift assays (EMSA) competition assays

2 μ M CA lattice was preloaded with increasing concentrations of refolded, unlabeled competitor RNAs (25–200 nM) in 1 \times binding buffer at 37°C for 10 min. A separate sample with 0 nM competitor was prepared in parallel to determine the maximum binding of aptamer CA15-2. A 10 \times annealing reaction containing 500 nM CA15-2 and 450 nM Cy5-labeled 56N reverse primer in 1X binding buffer underwent the same thermal renaturation and annealing described. The annealed CA15-2: Cy5-labeled 56N reverse primer complex was then added to the binding reaction to a 1 \times final concentration (50 nM CA15-2 and 45 nM Cy5-labeled 56N reverse primer) and incubated at 37°C for 15 min. 4 \times native loading dye (2 \times tris-borate [TB], 50% glycerol) was added to each reaction to a final concentration of 1 \times , and the samples were run on a 2% 0.5 \times TB-agarose gel at 8 V/cm. Gels were scanned for Cy5 fluorescence using the Typhoon FLA 9000 phosphorimager (GE Healthcare, Chicago, IL). The fraction of CA15-2 annealed to Cy5-labeled oligo retained in wells relative to No Competitor was quantified using Multi Gauge software (Fujifilm) using the following equation: (intensity of signal retained in well – intensity of signal in well of RNA only lane)/(intensity of signal retained in well of the no competitor lane – intensity of signal in well of RNA only lane). Experiments were performed in triplicate.

Nitrocellulose filter binding competition assays

To determine whether an unlabeled competitor was able to compete with 5'-radiolabeled CA15-2 for binding to the CA lattice, varying concentrations of unlabeled competitor (2.5–160 nM) were incubated with 250 nM CA lattice in 1 \times binding buffer at 37°C for 10 min. A separate sample with 0 nM competitor was prepared in parallel to determine the maximum binding of aptamer CA15-2. Unlabeled competitor RNAs (CA15-2, Arbitrary, Scrambled CA15-2, or yeast tRNA [Invitrogen, Carlsbad, CA]) were first refolded as described above. PF74 (Sigma Aldrich, St. Louis, MO) working stocks were prepared using a final concentration of 10% DMSO. 10 nM 5'-radiolabeled and refolded CA15-2 was then added to the binding reaction, which was incubated at 37°C for 15 min. Nitrocellulose filter binding assays were performed and the fraction of radiolabeled CA15-2 retained on the filter was calculated as described above. To calculate the relative % radiolabeled CA15-2 retained on filter, the fraction of radiolabeled CA15-2 retained on filter at each concentration of competitor was divided by the fraction radiolabeled CA15-2 retained on filter when no competitor was present (0 nM) and multiplied by 100%. The assays were done in triplicate.

To determine whether compound 15 was able to compete with 5'-radiolabeled aptamer CA15-2 prior to perform-

ing binding assays using compound 15-stabilized, assembled native CA lattice tubes, 10 μ M working stocks of compound 15 was prepared using a final concentration of 10% DMSO. 1 μ M unlabeled CA15-2 RNA or compound 15 was incubated with 1 μ M assembled CA lattice in 1 \times binding buffer for 10 min at 37°C. A separate sample with no competitor added was prepared in parallel to determine the maximum binding of aptamer CA15-2 to CA lattice. 50 nM 5'-radiolabeled and refolded CA15-2 was then added to the binding reaction, which was incubated at 37°C for 15 min. Nitrocellulose filter binding assays were performed as described and the fraction of radiolabeled CA15-2 retained on the filter was calculated as detailed above.

Microscale thermophoresis (MST)

The binding affinities of aptamer CA15-2 or the arbitrary RNA control for CA lattice, CA hexamer, and CA monomer were determined by measuring thermophoresis of Cy5-labeled RNAs in the presence of increasing concentrations of each individual capsid protein. Cy5-labeling of the RNAs was performed using the Label IT Nucleic Acid Labeling Kit according to the manufacturer's instructions (Mirus Bio, Madison, WI). Unreacted dye was removed using a Sephadex G-25 spin column provided with the kit. The ratio of RNA to dye was determined by measuring absorption at 260 nm for the RNA and 650 nm for the dye (molar absorbance: 250 000 M⁻¹ cm⁻¹). An average of 5 dye molecules were incorporated per RNA. Prior to performing MST experiments, nitrocellulose filter binding assays were performed as described above using the Cy5-labeled RNAs to ensure that Cy5 labeling did not alter the observed binding phenotypes. Reaction mixtures containing 100 nM Cy5-labeled aptamer CA15-2 or arbitrary RNA and increasing concentrations of the individual CA proteins (1–1000 nM) were prepared in binding buffer (50 mM Tris-HCl [pH 7.5], 100 mM KCl, 50 mM NaCl, 1 mM MgCl₂) containing 0.1% Pluoronic acid. Reaction mixtures were incubated for 30 min at room temperature and then loaded into capillaries. Thermophoresis was monitored on a Monolith NT.115 MST instrument (NanoTemper Technologies GmbH, Munich, Germany) at 20% LED power and high MST power with 20 s MST-on time, and data were analyzed with MO.Affinity software (version 2.3) using a 1:1 binding model (NanoTemper Technologies, CA). The final data were plotted using GraphPad Prism (Version 6.0) (GraphPad Inc., La Jolla, CA). Experiments were performed at least three times.

Producer cell assay

For experiments evaluating the effects of aptamer CA15-2 on a single cycle of HIV-1 replication at the producer cell stage (90,109), 293FT cells were co-transfected with pNL4-3-CMV-GFP (250 ng), pMD-G (100 ng) and aptamer- or non-binding RNA control-expressing plasmids at the indicated dosages using polyethylenimine (PEI; 1 μ l of 1 mg/ml PEI per μ g DNA). After 48 h, supernatants containing VSV-G-pseudotyped viruses produced in the presence of aptamers or controls were harvested. Cellular debris was removed by centrifugation and viral supernatants were frozen

at -80°C . Infectivity was determined by adding equal volumes of viral supernatant per sample to TZM-GFP cells such that the arbitrary RNA control infectivity levels were $\sim 10\%$. Infected cells were collected 48 h post-infection and fixed with 2% paraformaldehyde. The number of infected cells was determined by measuring the number of GFP-positive cells using an Accuri C6 Flow Cytometer (BD Biosciences, Franklin Lakes, NJ). The number of GFP-positive cells was normalized to p24 ELISA values and to the arbitrary RNA control to determine the relative infectivity for each sample. Biological replicates for these experiments were performed at least three times and each experiment included two technical replicates.

Target cell assay

For experiments evaluating the ability of aptamer CA15-2 or the arbitrary RNA control to protect cells from infection by pseudotyped HIV-1 particles (90), viruses were first produced in the absence of aptamer or controls by co-transfecting 293FT cells in 10 cm dishes with pNL4-3-CMV-GFP (250 ng) and pMD-G (100 ng) complexed with PEI. Virus was harvested 48 h post-transfection as described above. Separately, aptamer- or arbitrary RNA control-expressing plasmids (1000 ng) were transfected into fresh target 293FT cells using PEI. At 48 hr post-transfection, the aptamer- or control-expressing cells were challenged with virus produced in the absence of aptamer. Infected cells were harvested 48 hr later, fixed with 2% paraformaldehyde, and analyzed by flow cytometry for expression of EGFP as described above. Experiments were performed at least three times.

Data availability/sequence data resources

All aptamer sequences utilized in this work are listed in Table 1. The full sequence of the pcDNA3.1-based aptamer expression plasmid is available upon request.

Statistical analysis

To determine whether there was a statistically significant difference between two sets of samples, P values were calculated using an unpaired t test computed by GraphPad Prism.

Web sites/data base referencing

Structure prediction throughout this work was performed using the NUPACK web server (www.nupack.org) (117).

RESULTS AND DISCUSSION

Selection of RNA aptamers with affinity to the assembled HIV-1 CA lattice

The viral capsid core is a complex target that contains a variety of potential binding sites for aptamers and other novel ligands. Some of these sites are uniquely present in viral capsid cores because they lie at the junctions between hexamer or pentamer units; others are present within individual CA hexamers, pentamers, or monomers. However,

intact viral capsid cores are difficult to isolate with the purity and quantity required for aptamer selection. Therefore, we utilize an *in vitro* assembled, stabilized HIV-1 CA lattice (referred to here as CA lattice) as a surrogate for the lattice present within the viral capsid core (37). The A14C/E45C CA double mutant forms disulfide bonds between adjacent CA monomers within a hexamer, and these cross-linked hexamers assemble into hyperstabilized CA lattice tubes at high salt concentrations (Supplemental Figure S1B). Importantly, due to the cross-linking, these stabilized tubes can be removed from high salt buffers without disrupting the lattice and have been shown to maintain interactions with lattice-binding host factors (65). In addition, the CA lattice tubes can be pelleted by centrifugation, enabling partitioning of bound versus unbound RNAs during the aptamer selection process. Aptamer-targetable sites on the CA lattice include those present on the CA monomer, CA hexamer and/or CA lattice (Figure 1A).

To identify CA lattice-binding aptamers, the refolded 56N RNA library was incubated with CA lattice, followed by pelleting of CA lattice to partition bound versus unbound RNA sequences. Unbound sequences were discarded with the supernatant, while bound sequences were recovered from the pellet after washing. Recovered RNA was reverse transcribed and PCR amplified to restore the T7 RNA polymerase promoter (see Table 1). The resulting dsDNA was then used for *in vitro* transcription to generate the RNA library for the next round of selection (Figure 1B). A total of 15 rounds of selection were performed.

We determined the binding profiles of the RNA libraries from rounds 8, 10 and 15 to different HIV-1 CA assembly forms using nitrocellulose filter binding assays, including CA lattice (selection target), soluble CA monomer, and soluble CA hexamer (Supplemental Figure S1C). The CA monomer expression construct contains no mutations, while the soluble CA hexamer construct contains the same A14C/E45C mutations as the CA lattice, along with two additional alanine mutations (W184A/M185A) that abolish higher order lattice assembly (37). As expected, the three aptamer libraries exhibited dose-dependent binding to CA lattice as compared to the starting library (Figure 1C). In contrast, there was no significant change in dose-dependent binding of the aptamer libraries to either the CA monomer (Figure 1D) or CA hexamer (Figure 1E), indicating that most of the RNA species in these libraries recognize epitopes that are uniquely present on CA lattice.

Sanger sequencing of plasmids generated from cloning of Rounds 8, 10 and 15 (Table 1) did not reveal obvious convergence. However, in preliminary screens to evaluate binding of a subset of the individual clones to CA lattice (Supplemental Figure S2), aptamer CA15-2 consistently exhibited strong, dose-dependent binding to CA lattice, and we chose to focus on aptamer CA15-2 for further characterization.

Aptamer CA15-2 binds to the assembled CA lattice but not the soluble CA hexamer or CA monomer

Binding of aptamer CA15-2 to different CA protein assembly forms was evaluated using nitrocellulose filter binding assays, electrophoretic mobility shift assays (EMSA), microscale thermophoresis (MST), and size exclusion chro-

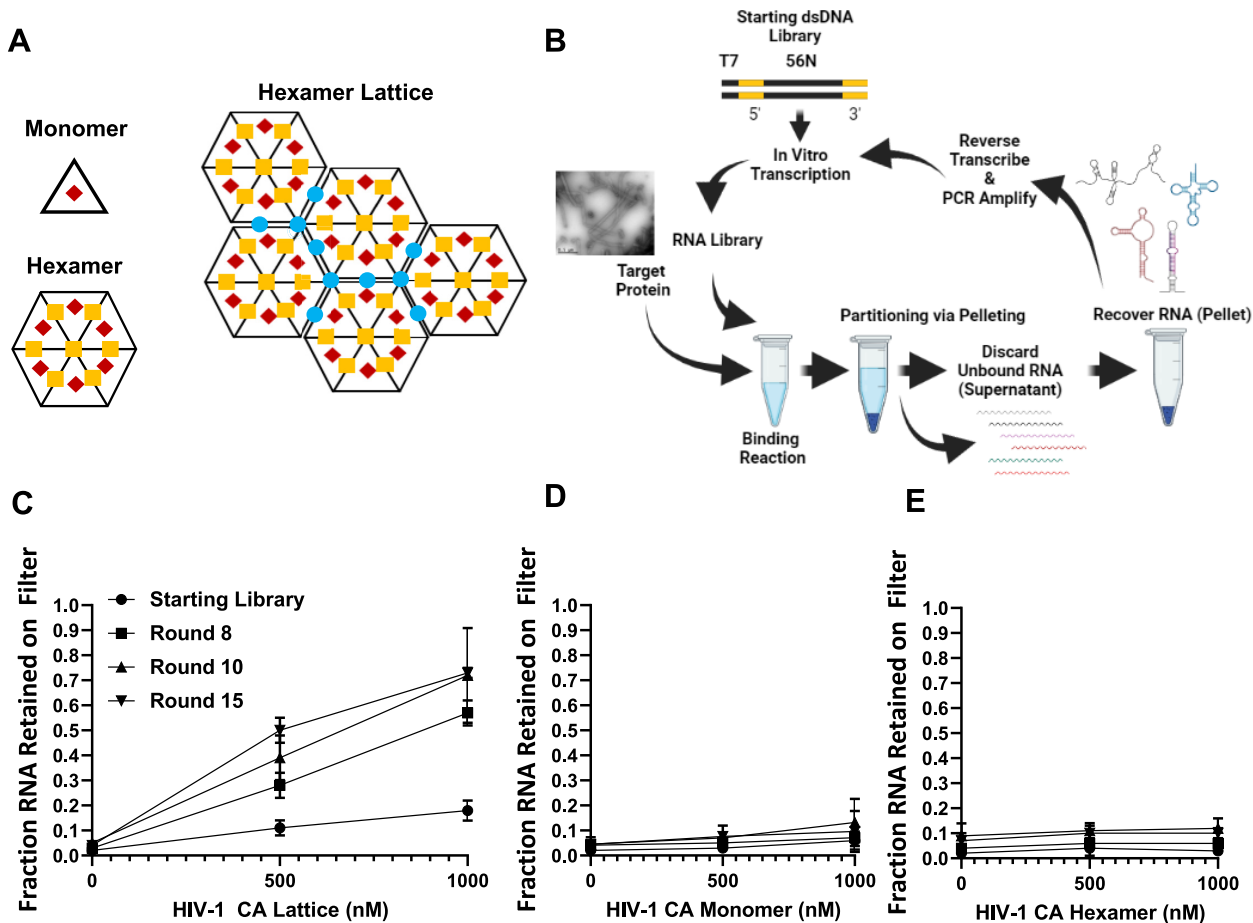


Figure 1. CA lattice aptamer selection. (A) Potential binding interfaces for CA-binding aptamers that are associated with the CA monomer (diamonds), CA hexamer (squares), and CA lattice (circles). (B) Schematic representation of the HIV-1 CA lattice aptamer selection created using BioRender.com. The starting dsDNA library containing the T7 promoter and a 56-nucleotide random region flanked by 5' and 3' constant regions was transcribed using T7 RNA polymerase. The RNA library was incubated with assembled HIV-1 CA lattice tubes (transmission electron microscopy image of the lattice tubes is shown) in a binding reaction. Library partitioning via pelleting was performed to separate the bound RNA (pellet) from the unbound RNA (supernatant). Bound RNA was recovered, reverse transcribed into cDNA, PCR-amplified, and transcribed to generate the RNA library to be used in the next round of selection. (C–E) Binding of aptamer libraries from rounds 8, 10 and 15 to the HIV-1 capsid lattice (C), CA monomer (D) and CA hexamer (E) was evaluated using nitrocellulose filter binding assays ($n = 3$). Binding for each library set was compared to the starting library for determination of statistical significance; ns ($P > 0.05$), ** ($P < 0.01$), *** ($P < 0.001$). Statistical significance for each round (500 and 1000 nM CA lattice) is as follows: Round 8 (**, ***), Round 10 (**, **) and Round 15 (***, ***). Throughout this study, CA concentrations for all assembly forms are given in terms of total monomer.

matography (SEC). The purity of each protein is represented in Supplemental Figure S1C. Aptamer CA15-2 exhibited a significant mobility shift in the presence of CA lattice via both EMSA (Figure 2A) and SEC (Supplemental Figure S3A). It also exhibited dose-dependent binding to CA lattice in nitrocellulose filter binding assays (Figure 2B and C) and MST assays (Figure 2D). In contrast, the arbitrary control RNA showed little or no interaction with CA lattice (Figure 2B–D and S3A) (109). Furthermore, aptamer CA15-2 showed no evidence of binding to CA monomer (Figure 2E and S3B) or to CA hexamer (Figure 2F and S3C) in contrast to positive control, PF74, which bound both the CA monomer and CA hexamer (data not shown). Collectively, these data demonstrate specificity of aptamer CA15-2 for CA lattice.

When binding of aptamer CA15-2 to the CA lattice was evaluated using nitrocellulose filter binding assays at a

wider range of CA protein concentrations (10–7500 nM), an apparent dissociation constant (K_{Dapp}) for aptamer CA15-2 was determined to be 502 ± 57 nM, while the apparent K_D for the arbitrary control was greater than $7.5 \mu\text{M}$ (Figure 2C). In a similar experiment performed using MST at a CA protein concentration range of 0.1–1000 nM, aptamer CA15-2 was observed to bind the HIV-1 CA lattice with an equilibrium dissociation constant of 350 ± 50 nM, while the arbitrary control demonstrated no binding (Figure 2D). Notably, the apparent K_D values obtained here may not be representative of the true CA-binding strength of aptamer CA15-2. Due to the heterogeneity of the CA lattice tubes, which likely contain varying numbers of binding sites depending on tube length and diameter, CA concentrations were calculated based on the total number of CA monomer (p24) present. Finally, to confirm aptamer CA15-2 binding to CA lattice,

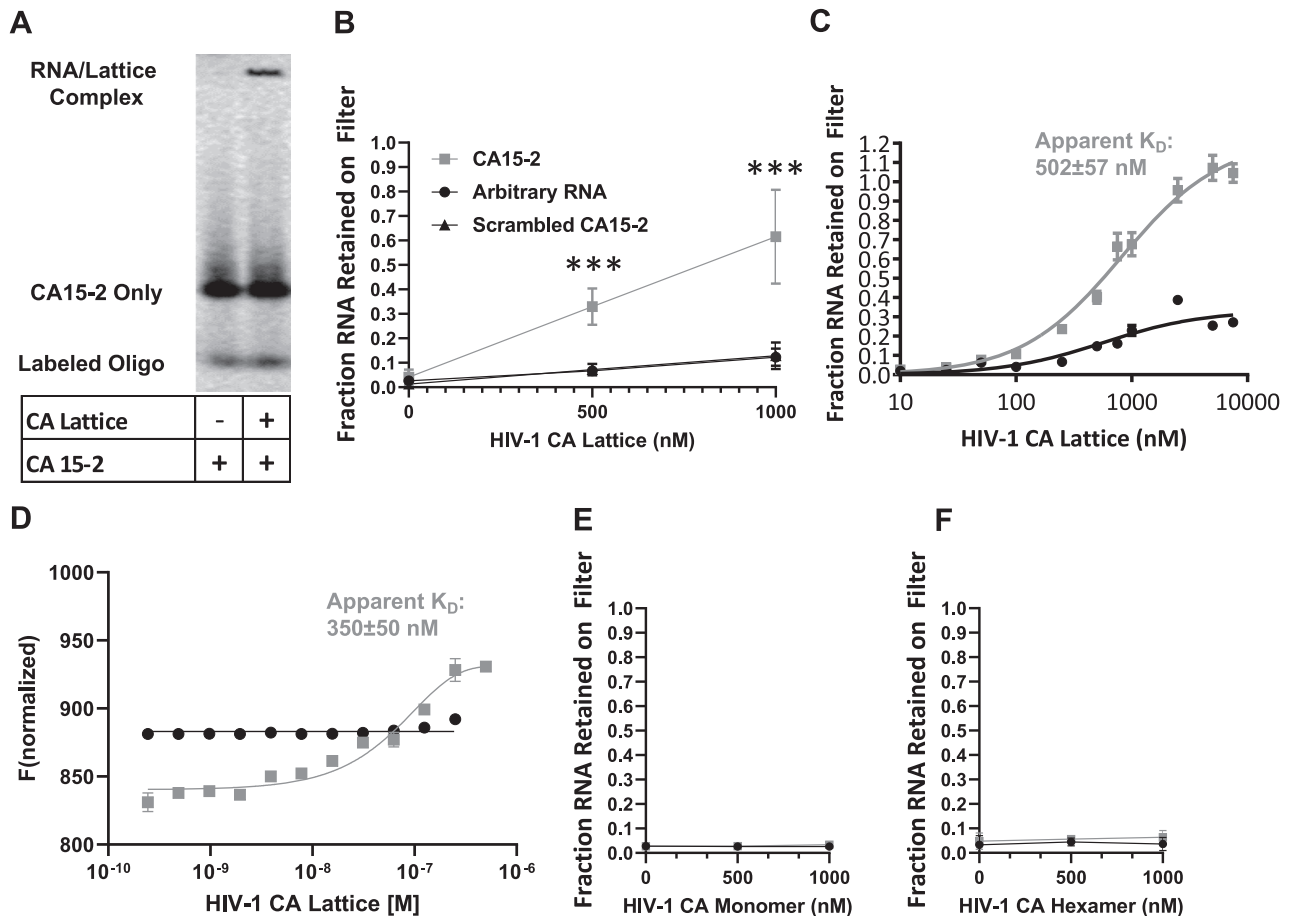


Figure 2. Specific binding of aptamer CA15-2 to the HIV-1 CA lattice. (A) An electrophoretic mobility shift assay demonstrates formation of a complex between Cy5-labeled aptamer CA15-2 and CA lattice. (B, C, E and F) Nitrocellulose filter binding assays were used to evaluate binding of radiolabeled aptamer CA15-2 or arbitrary RNA to the CA lattice (B and C; $n = 8$), hexamer (E; $n = 6$) and monomer (F; $n = 3$). Statistical comparisons were made between CA15-2 and the arbitrary control. *** ($P < 0.001$). (D) Microscale thermophoresis assays were used to confirm aptamer CA15-2 binding to the CA lattice using Cy5-labeled CA15-2 and the indicated concentrations of CA lattice.

we examined the aptamer-CA lattice complex using SEC, where we observed the retention volume of the complex to be ~ 7 ml as compared to ~ 15 ml for aptamer CA15-2 alone and ~ 20 ml for CA lattice alone (Supplemental Figure S3A). Collectively, these results demonstrate that aptamer CA15-2 specifically binds to CA lattice, likely at protein interfaces that are uniquely present on CA lattice but that are not present on the CA hexamer or CA monomer (Figure 1A).

Unlabeled CA15-2, but not other unlabeled nucleic acids, competes with labeled CA15-2 for binding to CA lattice

To confirm the binding specificity of aptamer CA15-2 to CA lattice, we performed competition assays using aptamer CA15-2 annealed to Cy5-labeled antisense oligonucleotide (EMSA) or radiolabeled aptamer CA15-2 (nitrocellulose filter binding assays) paired with a panel of unlabeled competitors. Unlabeled competitor was first incubated with CA lattice prior to addition of Cy5-labeled aptamer CA15-2. For the EMSA, 0–200 nM unlabeled competitor

was used, along with 50 nM aptamer CA15-2 and 2 μ M CA lattice. For the nitrocellulose filter binding assays, 0–160 nM unlabeled competitor was used with 10 nM aptamer CA15-2 and 250 nM CA lattice. The fraction of Cy5-labeled aptamer CA15-2 that bound in the absence and presence of increasing concentrations of unlabeled competitor was then compared to determine the impact of the competitor on the complex between aptamer CA15-2 and CA lattice. As expected, the relative amount of Cy5-labeled CA15-2 bound to CA lattice decreased as the concentration of unlabeled aptamer CA15-2 increased (Figure 3 and S4). Notably, the relative amount of labeled aptamer CA15-2 bound to CA lattice when unlabeled aptamer CA15-2 was present was significantly different from the amount present when unlabeled nonspecific RNAs were present in the binding reaction, even at the highest concentrations of unlabeled competitor. Unlabeled nonspecific RNAs used included Arbitrary RNA (Figure 3, S4 and S5A), a 3' truncation of Arbitrary RNA (Arbitrary 1–80nt; Figure 3 and S4), Scrambled CA15-2 (Figure 3, S4 and S5B), and yeast tRNA (Supplemental Figure S5C). These

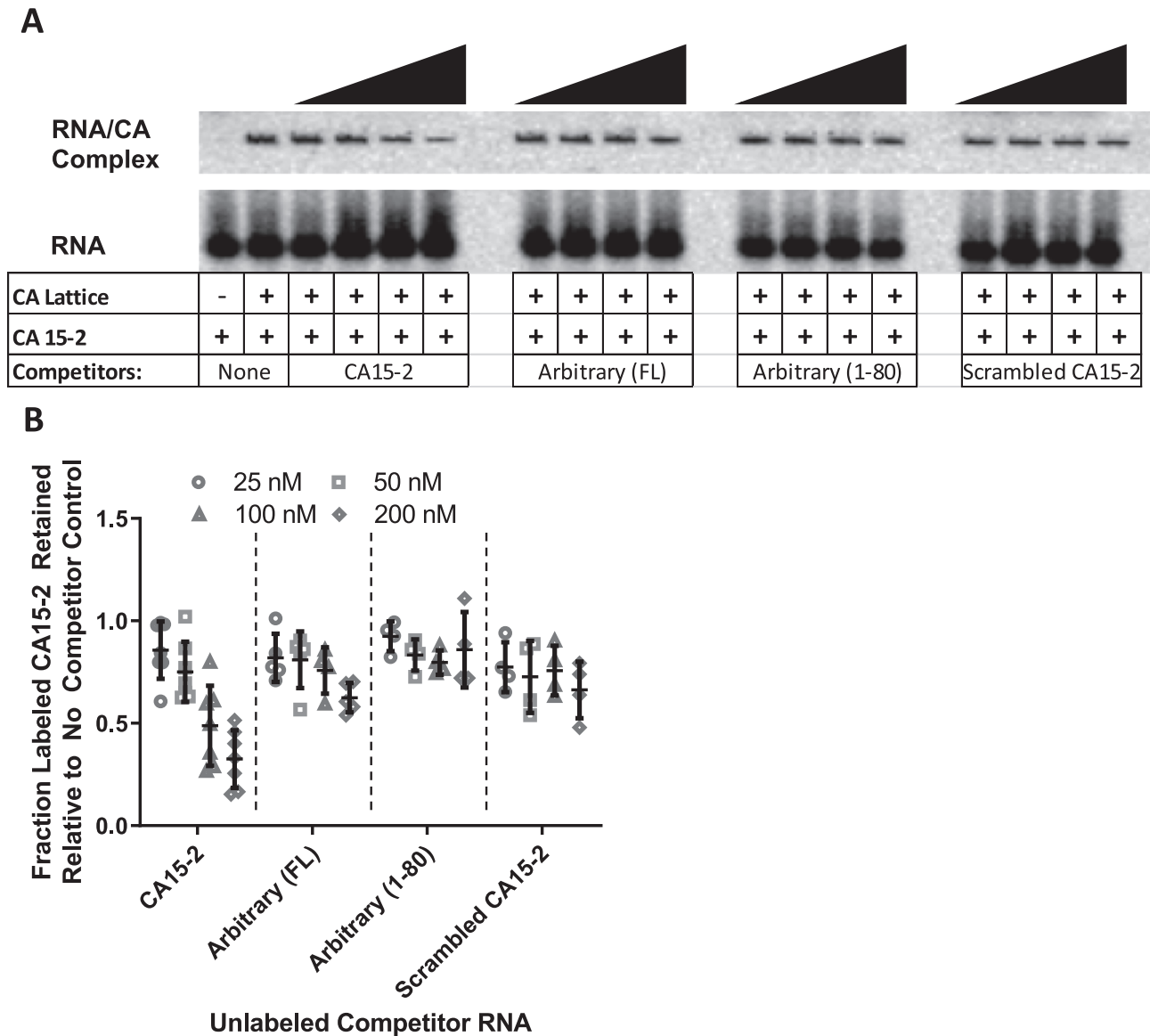


Figure 3. Competition of unlabeled competitors with Cy5-labeled aptamer CA15-2 for binding to CA lattice. (A) Electrophoretic mobility shift assays were used to determine the ability of unlabeled competitors to compete with Cy5-labeled aptamer CA15-2 for binding to the assembled CA lattice. Unlabeled full length CA15-2 was able to compete for binding to a greater degree than non-binding control RNAs (Arbitrary (FL), Arbitrary (1–80), and Scrambled CA15-2). (B) The fraction CA15-2 retained in wells relative to No Competitor was quantified using Multi Gauge software (Fujifilm) using the following equation: (intensity of signal retained in well – intensity of signal in well of RNA only lane)/(intensity of signal retained in well of No Competitor lane – intensity of signal in well of RNA only lane). Values are the mean \pm SD for three experiments.

results between specific and non-specific competitors are consistent with a model in which unlabeled aptamer CA15-2 blocks binding by labeled aptamer CA15-2 via saturation of specific interaction sites on CA lattice. Minimal competition was observed with all other non-specific RNAs in the nitrocellulose filter binding assay (Figure S5). The experiment utilized a low concentration of radiolabeled aptamer CA15-2, where binding would not be saturated. Thus, specific binding in this case would be lower than maximal binding. This is particularly relevant due to the possibility that binding affinity may be underrepresented by our apparent K_d determinations in Figure 2, as discussed above. Notably, defining the minimal binding structure of ap-

tamer CA15-2 may improve the observed apparent binding affinity.

We also evaluated competition between aptamer CA15-2 and PF74, a small molecule that inhibits HIV-1 replication (71,74,81) and that binds CA in a pocket located at the CA_{NTD}–CA_{CTD} interface of assembled hexamers with a K_d of 176 ± 78 nM (71). Radiolabeled aptamer CA15-2 did not compete with PF74 for binding to CA lattice at any of the concentrations tested (20–1280 nM; Supplemental Figure S5D), suggesting that aptamer CA15-2 does not share an overlapping binding site with PF74. This interpretation is further supported by the lack of binding observed for aptamer CA15-2 to CA hexamer (Figure 2E and S3B).

Involvement of the 3' and 5' constant regions of aptamer CA15-2 in binding to the CA lattice

The 56N library design included constant regions at the 5' and 3' ends for amplification during the selection process. To determine whether either constant region is required for aptamer CA15-2 binding to CA lattice, antisense oligonucleotides were separately annealed to each end of aptamer CA15-2 as represented in Figure 4A. The predicted CA15-2 structure was generated using NUPACK(117). After oligonucleotide annealing, binding to CA lattice was evaluated using nitrocellulose filter binding assays. Annealing of an antisense oligonucleotide to the 3' constant region did not significantly alter binding of aptamer CA15-2 to CA lattice as compared to the no oligonucleotide control (Figure 4B), indicating that sequestration via formation of a double-stranded region at the 3' end does not disrupt the proper folding of aptamer CA15-2 into a CA lattice-binding structure. In contrast, when an antisense oligonucleotide was annealed to the 5' constant region, binding to CA lattice was significantly decreased as compared to the no oligonucleotide control (Figure 4B). This indicates that sequestration of the 5' constant region via formation of a double stranded region interferes with the proper folding of aptamer CA15-2, ultimately blocking binding to CA lattice.

To further define the sequence requirements for aptamer CA15-2, we tested the ability of truncated aptamer variants to bind CA lattice. Structures for each variant were predicted using NUPACK (Supplemental Figure S6A–K) and the variants are named according to the nucleotides remaining after truncation. As shown in Figure 5A, full-length CA15-2 (1–104) and truncation 1–80 demonstrated significant binding to CA lattice in nitrocellulose assays ($P < 0.001$), consistent with the oligonucleotide annealing data above. Interestingly, truncation 25–104 also demonstrated significant binding, suggesting that the 5' constant region is not required for binding. Thus, the disruption of binding upon annealing of the 5' antisense oligonucleotide observed above (Figure 4B) may indicate that annealing introduced steric hinderance that disrupted the binding structure. Notably, binding was abolished in truncation 25–80, which removes both the 5' and 3' constant regions. This suggests that while there is not a specific requirement for either constant region, each constant region can contribute to the functional binding structure in the absence of the other.

Interestingly, truncation 1–60 demonstrated a greater degree of binding as compared to truncation 1–70 (Figure 5A; $P < 0.001$). These results were corroborated by EMSA-based competition assays, wherein the full-length aptamer (1–104) and truncations 1–80 and 1–60 competed with full-length CA15-2 for binding, as shown by the decrease in mobility shift with increasing competitor concentration (Figure 5C and S6). It is possible that 1–60 generates a stabilized structure capable of binding CA lattice, albeit to a lesser degree than 1–104 or 1–80, which may not be formed by 1–70. Truncations 1–50, 1–40, 25–80, 25–60 and 30–60 did not bind significantly over the arbitrary control (Figure 5A).

The predicted secondary structures of all active truncations of aptamer CA15-2 include a stem-loop structure from approximately position 25–62. We tested the importance of this stem by either disrupting the stem (1-80*) or

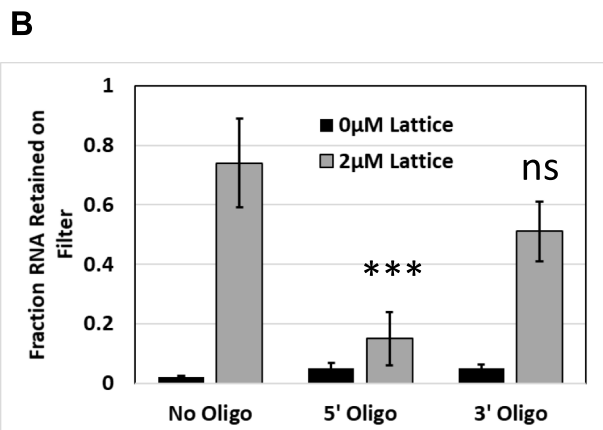
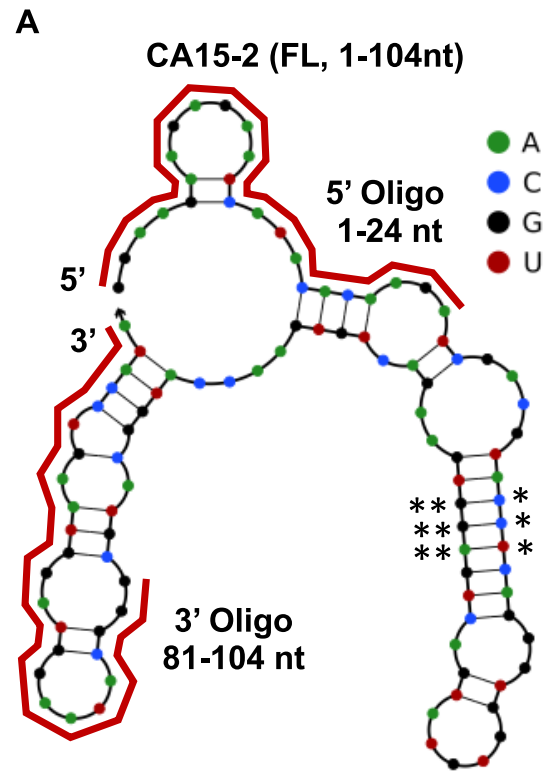
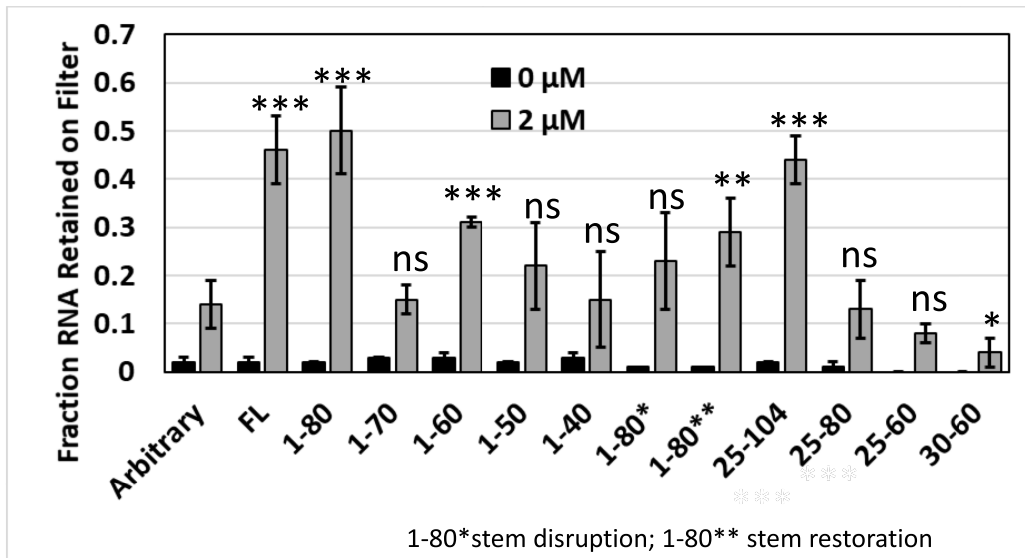


Figure 4. Contributions of the 5' and 3' constant regions to aptamer CA15-2 binding to the CA lattice via antisense oligonucleotide annealing. (A) The secondary structure of aptamer CA15-2 was predicted using the NUPACK web server (117). Red lines indicate binding sites for anti-sense oligonucleotides used to sequester the 5' and 3' constant regions. Asterisks indicate the location of stem disruption or stem restoration mutations evaluated in Figure 5. (B) Antisense oligonucleotides were annealed to either the 5' or 3' constant regions of aptamer CA15-2, followed by binding analysis using nitrocellulose filter assays. Statistical comparisons were made against the binding values for the arbitrary control. Values are the mean \pm SD for three experiments.

restoring the stem (1-80**) (Figure 4A (asterisks), 5A, and 5B (yellow highlight)). Disruption of the stem resulted in binding that was not statistically different from the arbitrary control, whereas restoration of the stem demonstrated significant binding ($P < 0.01$) as compared to the arbitrary control (Figure 5A). However, there was not a significant difference in binding between the disrupted stem and the

A



B

CA15-2

UCGACGUACCUCAGGGUGGUGUAUGACUGAGGUGAAGACUGUGAACCAUGGCAUGC

CA15-2 Stem Disrupt (1-80*)

UCGACGUAGAGCAGGGUGGUGUAUGACUGAGGUGAAGACUGUGAACCAUGGCAUGC

CA15-2 Stem Restore (1-80**)

UCGACGUAGAGCAGGGUGGUGUAUGACUGCUCUGAAGACUGUGAACCAUGGCAUGC

C

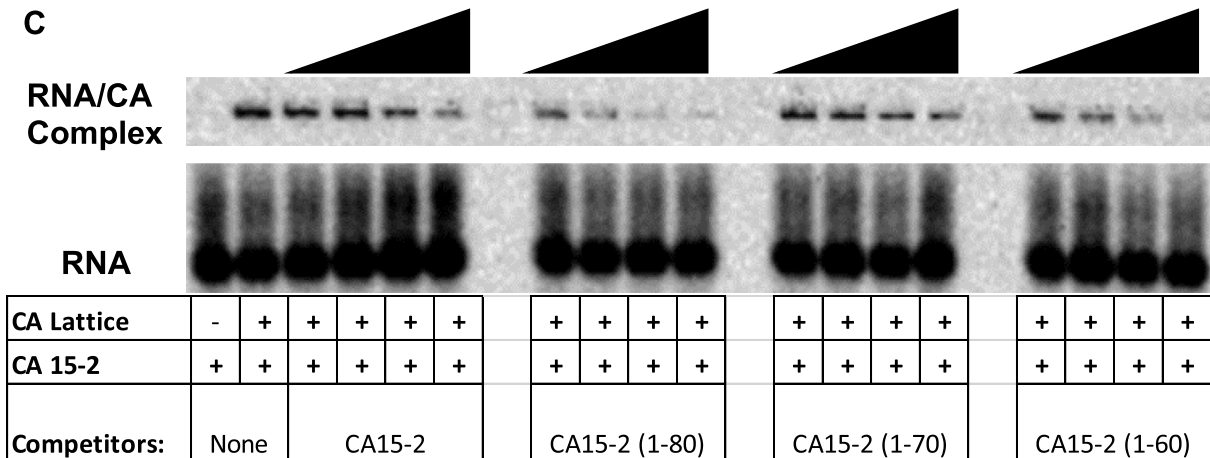


Figure 5. Contributions of the 5' and 3' constant regions to aptamer CA15-2 binding to CA lattice via truncations. Binding of aptamer CA15-2 and various truncations of aptamer CA15-2 was evaluated using nitrocellulose filter binding assays (A) and electrophoretic mobility shift assays (B). (A) Aptamers or control RNAs were radiolabeled, incubated with CA lattice, and evaluated using nitrocellulose filter binding assays. Values are the mean \pm SD for three experiments. Statistical comparisons were made for each truncation versus the level of binding for the arbitrary control. ns ($P > 0.05$), *** ($P < 0.001$). (B) Mutations introduced for disruption or restoration of a predicted stem structure in CA15-2 are shown in yellow. (C) Electrophoretic mobility shift assays were used to determine the ability of unlabeled truncated aptamers to compete with Cy5-labeled aptamer CA15-2 for binding to CA lattice. The fraction of Cy5-labeled, full-length aptamer CA15-2 retained in wells relative to No Competitor was quantified using Multi Gauge software (Fujifilm) using the following equation: (intensity of signal retained in well – intensity of signal in well of RNA only lane)/(intensity of signal retained in well of No Competitor lane – intensity of signal in well of RNA only lane). Experiments were repeated three times.

restored stem, and restoration of the stem did not restore binding to the level of 1–80. Thus, aptamer CA15-2 likely adopts a different structure than predicted by NUPACK or has specific nucleotide requirements. Collectively, these data suggest that the nucleotides required for aptamer binding reside within nucleotides 1–60, as the truncated aptamer (1–60) retained binding activity, albeit to a lower extent. The reduction of target affinity displayed by 1–60 is consistent with previous reports (118). Notably, our results also suggest that additional residues located within nucleotides 80–104 also play an important role, either by stabilizing the active fold or through additional contacts with the target molecule.

Aptamer CA15-2 binds native CA lattice tubes

Aptamer CA15-2 was selected against CA lattice containing mutations A14C/E45C. To determine whether these mutations were required for binding, we sought to evaluate binding to native CA lattice tubes. Common methods for assembly of native tubes rely on inclusion of IP6 or high concentrations of salt; however, these conditions abolished aptamer CA15-2 binding (Supplemental Figure S7). PF74 analog, compound 15, provides stabilization to allow for assembly of native CA tubes under physiological salt conditions (Supplemental Figure S8A). As we previously demonstrated that PF74 is unable to compete with aptamer CA15-2 for binding (Supplemental Figure S5D), we performed similar competition experiments with compound 15, followed by binding assays using native CA lattice tubes assembled in the presence of compound 15. As shown in Supplemental Figure S8, compound 15 is unable to compete with aptamer CA15-2 for binding to the assembled CA lattice (Supplemental Figure S8B) and aptamer CA15-2 is able to bind assembled native CA lattice tubes significantly over the arbitrary control, similarly to the assembled CA lattice used in the selection (Supplemental Figure S8C). These results demonstrate that binding of aptamer CA15-2 is not dependent upon the presence of the A14C/E45C mutations.

Aptamer CA15-2 inhibits HIV-1 infectivity at the producer cell stage but not at the target cell stage

To investigate whether intracellular expression of aptamer CA15-2 affects HIV-1 replication, we performed single-cycle infectivity assays using VSV-G-pseudotyped HIV-1 as previously described (109). In principle, such effects could occur during the efferent phase of the viral replication cycle (virus assembly and release) or the afferent phase (entry and infection). To examine these stages separately, we first determined the effect of aptamer CA15-2 during virus production by producing VSV-G-pseudotyped HIV-1 particles in cells that expressed either aptamer CA15-2 or the arbitrary RNA control (Figure 6A). Aptamer or arbitrary control RNA-expressing plasmids were co-transfected into 293FT cells along with the proviral plasmid, pNL4-3-CMV-EGFP and pMD-G which expresses VSV-G. Viruses were harvested 48 hr post infection and were used to infect fresh, non-aptamer-expressing TZM-GFP target cells. TZM-GFP cells produce GFP upon infection, increasing the intensity of the GFP signal. Total virus production, as measured by p24 ELISA, was slightly elevated for aptamer-

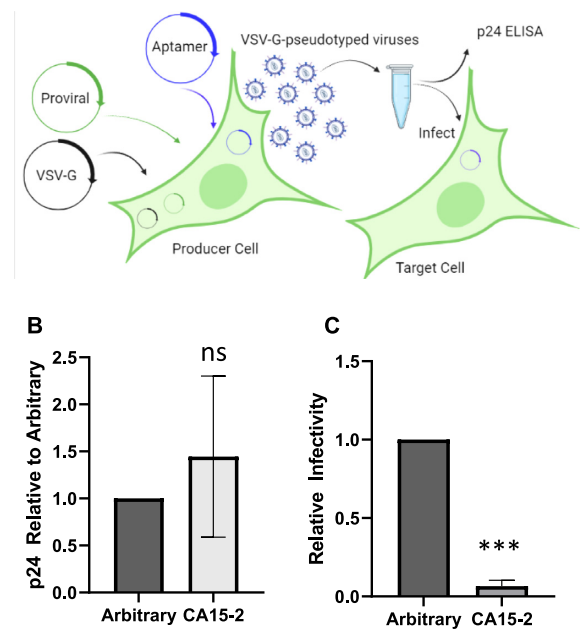


Figure 6. Aptamer CA15-2 effects on HIV-1 replication in producer cells. (A) Schematic depiction of the producer cell assay to evaluate aptamer effects when present during virus production created using BioRender.com. (B) p24 amounts were determined using ELISA for each sample and normalized to the arbitrary control for comparison. (C) Viral supernatants generated in aptamer-expressing cells were used to infect fresh TZM-GFP cells. Relative infectivity was determined by normalizing the percentage of EGFP positive cells to the amount of p24 present in each sample, followed by normalization to the arbitrary control. Values are the mean \pm SD for five experiments.

expressing cells, but the difference was not statistically significant (Figure 6B). In contrast, relative infectivity, as measured by the percentage of EGFP-positive cells normalized to p24 and the arbitrary control, was more than five-fold lower for aptamer CA15-2 compared to the arbitrary control (Figure 6C). Collectively, these results demonstrate that aptamer CA15-2 inhibits virus replication as compared to the arbitrary control when present during virus production and that these effects are not due to a decrease in viral particle release.

In contrast with the producer cell assay, we did not observe any reduction in infectivity when 293FT cells were first transfected with plasmids that expressed aptamer CA15-2 or the arbitrary control RNA prior to challenge with VSV-G-pseudotyped virus produced in the absence of aptamer (Figure 7). These results suggest that aptamer CA15-2 is unable to protect cells from incoming virus infection at the dose of aptamer used here. It is possible that aptamer CA15-2 can interact with the incoming viral capsid core, but that these interactions do not significantly impact post-entry steps of replication or capsid core stability. Alternatively, aptamer CA15-2 may not be present in a cellular location that enables interaction in target cells or may interact with a binding interface that is either not present or not accessible on the incoming viral capsid core but that is present and accessible during or after virus assembly in the producer cell.

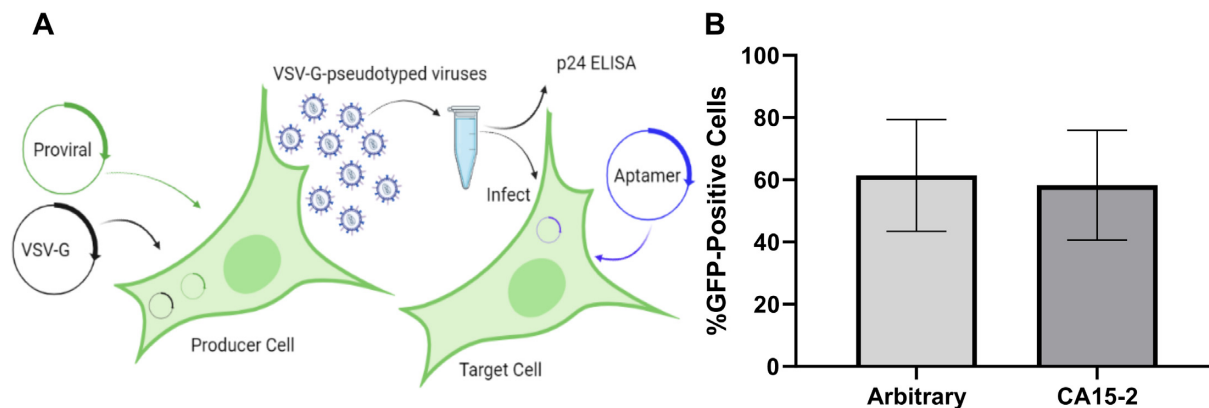


Figure 7. Aptamer CA15-2 effects on HIV-1 replication in target cells. (A) Schematic depiction of the target cell assay to evaluate aptamer effects on incoming virus created using BioRender.com. (B) Viral supernatants generated in the absence of aptamer were used to infect 293FT cells transfected for 48 h with plasmids for expression of the arbitrary control or CA15-2. Infectivity was determined by flow cytometry analysis of the number of EGFP-positive cells in each sample. Values are the mean \pm SD for three experiments.

There are many possibilities for the mechanism underlying the antiviral activity of CA15-2, on which we speculate here. As the level of p24 in the viral supernatant was similar in aptamer CA15-2 and the control samples, the defect does not appear to manifest in altered production of viral particles. It is possible that aptamer CA15-2 may impact genome packaging, virus assembly, encapsidation of a necessary host factor, virus maturation, or capsid stability, all of which are important for virus infectivity and would impact the ability of the virus to perform downstream replication steps. Recent work has suggested that the immature lattice is formed via recruitment of Gag dimers to the site of assembly to form hexamers, which then assemble into the immature lattice (53). We have demonstrated here that aptamer CA15-2 binds specifically to CA lattice but not to CA monomer or CA hexamer assembly forms. If the assembling immature lattice is available and accessible within the cell during virus production, it is possible that aptamer CA15-2 interacts with the assembling immature lattice. This interaction could drive specific incorporation of CA15-2 into viral particles, where CA15-2 could redirect the assembly process, resulting in defective viral particles. Alternatively, aptamer CA15-2 could be non-specifically incorporated into particles, providing an opportunity to interact with the lattice during remodeling that occurs as part of viral maturation to redirect the assembly process, leading to the replication defect. Indeed, we have previously demonstrated that, at the dosage of aptamer expression plasmid utilized in these experiments, aptamers, including non-binding controls, can be non-specifically encapsidated into viral particles (90). Further experiments are needed to elucidate these potential mechanisms.

Conclusions on CA lattice-targeting aptamers as new tools for interrogating the role of CA in HIV-1 replication

Aptamers offer several advantages over small molecules and antibodies in that they can fold into a variety of different structures, can be selected to display increased target affinity and specialized binding characteristics, and be easily mod-

ified for a variety of applications. In the case of RNA aptamers, specifically, they can also be expressed in cells as RNA transcripts. These advantages allow aptamers to engage in a variety of binding mechanisms, to outcompete other binding interactions, to achieve proper cellular localization, and to aid in visualization of cellular processes. Recent developments in our understanding of HIV-1 assembly and CA structure, as well as the availability of stabilized CA lattice tubes, provided a unique opportunity for the identification of aptamers capable of selectively binding the CA lattice. The work presented here details the successful selection of aptamers that bind CA lattice. We further characterized aptamer CA15-2, which binds CA lattice, but not CA monomer or CA hexamer, suggesting that aptamer CA15-2 binds an interface that is present on CA lattice, but not on CA monomer or CA hexamer. We found that aptamer CA15-2 was able to inhibit viral replication when expressed in producer cells, but not when expressed in target cells, opening the door to further examination of the mechanisms underlying viral inhibition by aptamer CA15-2. Aptamer CA15-2 and other aptamer clones from the same aptamer population represent new tools for discrimination of CA lattice from other CA assembly forms. Importantly, aptamers that recognize accessible sites specific to CA lattice or other CA assembly forms provide an opportunity to investigate impact of these interactions on diverse steps of HIV-1 replication, to further examine CA interactions with host factors, and to identify potentially novel interaction surfaces present on CA assembly forms, all of which could increase our understanding of viral biology and inform development of therapeutics.

SUPPLEMENTARY DATA

Supplementary Data are available at NAR Online.

ACKNOWLEDGEMENTS

We would like to acknowledge the following individuals for their technical and conceptual contributions to this work: Dr Marc Johnson, Dr Xiao Heng, Dr Owen Pornillos,

Dr Barbie Ganser-Pornillos, Dr David Porciani, Dr Kamlendra Singh, Dr Karen Kirby, and Qiongying (Grace) Yang.

FUNDING

National Institutes of Health [AI127195 to M.L., S.S., AI120860 to S.S.]; University of Missouri Life Sciences Fellowship (to P.G.); Wayne L. Ryan Graduate Fellowship from the Ryan Foundation (to P.G.). Funding for open access charge: generous startup funds provided to Dr Lange by the University of Missouri.

Conflict of interest statement. None declared.

REFERENCES

- Campbell, E.M. and Hope, T.J. (2015) HIV-1 capsid: the multifaceted key player in HIV-1 infection. *Nat. Rev. Microbiol.*, **13**, 471–483.
- Christensen, D.E., Ganser-Pornillos, B.K., Johnson, J.S., Pornillos, O. and Sundquist, W.I. (2020) Reconstitution and visualization of HIV-1 capsid-dependent replication and integration in vitro. *Science*, **370**, eabc8420.
- Fassati, A. (2012) Multiple roles of the capsid protein in the early steps of HIV-1 infection. *Virus Res*, **170**, 15–24.
- Sundquist, W.I. and Krausslich, H.G. (2012) HIV-1 assembly, budding, and maturation. *Cold Spring Harb. Perspect. Med.*, **2**, a006924.
- Rihn, S.J., Wilson, S.J., Loman, N.J., Alim, M., Bakker, S.E., Bhella, D., Gifford, R.J., Rixon, F.J. and Bieniasz, P.D. (2013) Extreme genetic fragility of the HIV-1 capsid. *PLoS Pathogens*, **9**, e1003461.
- Le Sage, V., Moulard, A.J. and Valiente-Echeverria, F. (2014) Roles of HIV-1 capsid in viral replication and immune evasion. *Virus Res.*, **193**, 116–129.
- James, L.C. (2019) The HIV-1 capsid: more than just a delivery package. *Adv. Exp. Med. Biol.*, **1215**, 69–83.
- Novikova, M., Zhang, Y., Freed, E.O. and Peng, K. (2019) Multiple roles of HIV-1 capsid during the virus replication cycle. *Virol. Sin.*, **34**, 119–134.
- Forshey, B.M., von Schwedler, U., Sundquist, W.I. and Aiken, C. (2002) Formation of a human immunodeficiency virus type 1 core of optimal stability is crucial for viral replication. *J. Virol.*, **76**, 5667–5677.
- Eschbach, J.E., Elliott, J.L., Li, W., Zdrozny, K.K., Davis, K., Mohammed, S.J., Lawson, D.Q., Pornillos, O., Engelman, A.N. and Kutluay, S.B. (2020) Capsid lattice destabilization leads to premature loss of the viral genome and integrase enzyme during HIV-1 infection. *J. Virol.*, **95**, e00984-20.
- Rossi, E., Meuser, M.E., Cunanan, C.J. and Cocklin, S. (2021) Structure, function, and interactions of the HIV-1 capsid protein. *Life (Basel)*, **11**, 100.
- Summers, B.J., Digianantonio, K.M., Smaga, S.S., Huang, P.T., Zhou, K., Gerber, E.E., Wang, W. and Xiong, Y. (2019) Modular HIV-1 capsid assemblies reveal diverse host-capsid recognition mechanisms. *Cell Host Microbe*, **26**, 203–216.
- Naghavi, M.H. (2021) HIV-1 capsid exploitation of the host microtubule cytoskeleton during early infection. *Retrovirology*, **18**, 19.
- Zhuang, S. and Torbett, B.E. (2021) Interactions of HIV-1 capsid with host factors and their implications for developing novel therapeutics. *Viruses*, **13**, 417.
- Mascarenhas, A.P. and Musier-Forsyth, K. (2009) The capsid protein of human immunodeficiency virus: interactions of HIV-1 capsid with host protein factors. *FEBS J*, **276**, 6118–6127.
- Burdick, R.C., Delviks-Frankenberry, K.A., Chen, J., Janaka, S.K., Sastri, J., Hu, W.S. and Pathak, V.K. (2017) Dynamics and regulation of nuclear import and nuclear movements of HIV-1 complexes. *PLoS Pathog*, **13**, e1006570.
- Achuthan, V., Pereira, J.M., Ahn, J.J., Brass, A.L. and Engelman, A.N. (2019) Capsid-CPSF6 interaction: master regulator of nuclear HIV-1 positioning and integration. *J. Life Sci (Westlake Village)*, **1**, 39–45.
- Francis, A.C., Marin, M., Prellberg, M.J., Palermino-Rowland, K. and Melikyan, G.B. (2020) HIV-1 uncoating and nuclear import precede the completion of reverse transcription in cell lines and in primary macrophages. *Viruses*, **12**, 1234.
- Selyutina, A., Persaud, M., Lee, K., KewalRamani, V. and Diaz-Griffero, F. (2020) Nuclear import of the HIV-1 core precedes reverse transcription and uncoating. *Cell Rep.*, **32**, 108201.
- Blanco-Rodriguez, G. and Di Nunzio, F. (2021) The viral capsid: a master key to access the host nucleus. *Viruses*, **13**, 1178.
- Dharan, A., Bachmann, N., Talley, S., Zwickelmaier, V. and Campbell, E.M. (2020) Nuclear pore blockade reveals that HIV-1 completes reverse transcription and uncoating in the nucleus. *Nat. Microbiol.*, **5**, 1088–1095.
- Burdick, R.C., Li, C., Munshi, M., Rawson, J.M.O., Nagashima, K., Hu, W.S. and Pathak, V.K. (2020) HIV-1 uncoats in the nucleus near sites of integration. *Proc. Natl. Acad. Sci. U.S.A.*, **117**, 5486–5493.
- Muller, T.G., Zila, V., Peters, K., Schifferdecker, S., Stanic, M., Lucic, B., Laketa, V., Lusic, M., Muller, B. and Krausslich, H.G. (2021) HIV-1 uncoating by release of viral cDNA from capsid-like structures in the nucleus of infected cells. *Elife*, **10**, e64776.
- Li, C., Burdick, R.C., Nagashima, K., Hu, W.S. and Pathak, V.K. (2021) HIV-1 cores retain their integrity until minutes before uncoating in the nucleus. *Proc. Natl. Acad. Sci. U.S.A.*, **118**, e2019467118.
- Zila, V., Margiotta, E., Turonova, B., Muller, T.G., Zimmerli, C.E., Mattei, S., Allegretti, M., Borner, K., Rada, J., Muller, B. et al. (2021) Cone-shaped HIV-1 capsids are transported through intact nuclear pores. *Cell*, **184**, 1032–1046.
- Takemura, T. and Murakami, T. (2012) Functional constraints on HIV-1 capsid: their impacts on the viral immune escape potency. *Front. Microbiol.*, **3**, 369.
- Grutter, M.G. and Luban, J. (2012) TRIM5 structure, HIV-1 capsid recognition, and innate immune signaling. *Curr. Opin. Virol.*, **2**, 142–150.
- Sultana, T., Mamede, J.I., Saito, A., Ode, H., Nohata, K., Cohen, R., Nakayama, E.E., Iwatani, Y., Yamashita, M., Hope, T.J. et al. (2019) Multiple pathways to avoid beta interferon sensitivity of HIV-1 by mutations in capsid. *J. Virol.*, **93**, e00986-19.
- Pornillos, O. and Ganser-Pornillos, B.K. (2019) Maturation of retroviruses. *Curr. Opin. Virol.*, **36**, 47–55.
- Kucharska, I., Ding, P., Zdrozny, K.K., Dick, R.A., Summers, M.F., Ganser-Pornillos, B.K. and Pornillos, O. (2020) Biochemical reconstitution of HIV-1 assembly and maturation. *J. Virol.*, **94**, e01844-19.
- Tsiang, M., Niedziela-Majka, A., Hung, M., Jin, D., Hu, E., Yant, S., Samuel, D., Liu, X. and Sakowicz, R. (2012) A trimer of dimers is the basic building block for human immunodeficiency virus-1 capsid assembly. *Biochemistry*, **51**, 4416–4428.
- Worthylake, D.K., Wang, H., Yoo, S., Sundquist, W.I. and Hill, C.P. (1999) Structures of the HIV-1 capsid protein dimerization domain at 2.6 Å resolution. *Acta Crystallogr. D Biol. Crystallogr.*, **55**, 85–92.
- Ganser-Pornillos, B.K., Cheng, A. and Yeager, M. (2007) Structure of full-length HIV-1 CA: a model for the mature capsid lattice. *Cell*, **131**, 70–79.
- Pornillos, O., Ganser-Pornillos, B.K., Kelly, B.N., Hua, Y., Whitby, F.G., Stout, C.D., Sundquist, W.I., Hill, C.P. and Yeager, M. (2009) X-ray structures of the hexameric building block of the HIV capsid. *Cell*, **137**, 1282–1292.
- Byeon, I.J., Meng, X., Jung, J., Zhao, G., Yang, R., Ahn, J., Shi, J., Concel, J., Aiken, C., Zhang, P. et al. (2009) Structural convergence between Cryo-EM and NMR reveals intersubunit interactions critical for HIV-1 capsid function. *Cell*, **139**, 780–790.
- von Schwedler, U.K., Stray, K.M., Garrus, J.E. and Sundquist, W.I. (2003) Functional surfaces of the human immunodeficiency virus type 1 capsid protein. *J. Virol.*, **77**, 5439–5450.
- Pornillos, O., Ganser-Pornillos, B.K., Banumathi, S., Hua, Y. and Yeager, M. (2010) Disulfide bond stabilization of the hexameric capsomer of human immunodeficiency virus. *J. Mol. Biol.*, **401**, 985–995.
- Meng, X., Zhao, G. and Zhang, P. (2011) Structure of HIV-1 capsid assemblies by cryo-electron microscopy and iterative helical real-space reconstruction. *J. Vis. Exp.*, **54**, 3041.
- Zhao, G., Perilla, J.R., Yufenyuy, E.L., Meng, X., Chen, B., Ning, J., Ahn, J., Gronenborn, A.M., Schulten, K., Aiken, C. et al. (2013)

- Mature HIV-1 capsid structure by cryo-electron microscopy and all-atom molecular dynamics. *Nature*, **497**, 643–646.
40. Gres, A.T., Kirby, K.A., KewalRamani, V.N., Tanner, J.J., Pornillos, O. and Sarafianos, S.G. (2015) STRUCTURAL VIROLOGY. X-ray crystal structures of native HIV-1 capsid protein reveal conformational variability. *Science*, **349**, 99–103.
 41. Cortines, J.R., Lima, L.M., Mohana-Borges, R., Millen Tde, A., Gaspar, L.P., Lanman, J.K., Prevelige, P.E. Jr and Silva, J.L. (2015) Structural insights into the stabilization of the human immunodeficiency virus type 1 capsid protein by the cyclophilin-binding domain and implications on the virus cycle. *Biochim. Biophys. Acta*, **1854**, 341–348.
 42. Wacharapornin, P., Lauhakirti, D. and Auewarakul, P. (2007) The effect of capsid mutations on HIV-1 uncoating. *Virology*, **358**, 48–54.
 43. Yu, X., Wang, Q., Yang, J.C., Buch, I., Tsai, C.J., Ma, B., Cheng, S.Z., Nussinov, R. and Zheng, J. (2009) Mutational analysis and allosteric effects in the HIV-1 capsid protein carboxyl-terminal dimerization domain. *Biomacromolecules*, **10**, 390–399.
 44. Manochewa, S., Swain, J.V., Lanxon-Cookson, E., Rolland, M. and Mullins, J.I. (2013) Fitness costs of mutations at the HIV-1 capsid hexamerization interface. *PLoS One*, **8**, e66065.
 45. Yufenyuy, E.L. and Aiken, C. (2013) The NTD-CTD intersubunit interface plays a critical role in assembly and stabilization of the HIV-1 capsid. *Retrovirology*, **10**, 29.
 46. Hulme, A.E., Kelley, Z., Okocha, E.A. and Hope, T.J. (2015) Identification of capsid mutations that alter the rate of HIV-1 uncoating in infected cells. *J. Virol.*, **89**, 643–651.
 47. Bayro, M.J., Chen, B., Yau, W.M. and Tycko, R. (2014) Site-specific structural variations accompanying tubular assembly of the HIV-1 capsid protein. *J. Mol. Biol.*, **426**, 1109–1127.
 48. Lampel, A., Bram, Y., Ezer, A., Shaltiel-Kario, R., Saad, J.S., Bacharach, E. and Gazit, E. (2015) Targeting the early step of building block organization in viral capsid assembly. *ACS Chem. Biol.*, **10**, 1785–1790.
 49. Lampel, A., Varenik, M., Regev, O. and Gazit, E. (2015) Hierarchical multi-step organization during viral capsid assembly. *Colloids Surf. B Biointerfaces*, **136**, 674–677.
 50. Hulme, A.E., Kelley, Z., Foley, D. and Hope, T.J. (2015) Complementary assays reveal a low level of CA associated with viral complexes in the nuclei of HIV-1-infected cells. *J. Virol.*, **89**, 5350–5361.
 51. Dismuke, D.J. and Aiken, C. (2006) Evidence for a functional link between uncoating of the human immunodeficiency virus type 1 core and nuclear import of the viral preintegration complex. *J. Virol.*, **80**, 3712–3720.
 52. Ganser-Pornillos, B.K., Yeager, M. and Pornillos, O. (2012) Assembly and architecture of HIV. *Adv. Exp. Med. Biol.*, **726**, 441–465.
 53. Tan, A., Pak, A.J., Morado, D.R., Voth, G.A. and Briggs, J.A.G. (2021) Immature HIV-1 assembles from Gag dimers leaving partial hexamers at lattice edges as potential substrates for proteolytic maturation. *Proc. Natl. Acad. Sci. U.S.A.*, **118**, e2020054118.
 54. Mattei, S., Glass, B., Hagen, W.J., Krausslich, H.G. and Briggs, J.A. (2016) The structure and flexibility of conical HIV-1 capsids determined within intact virions. *Science*, **354**, 1434–1437.
 55. Perilla, J.R. and Gronenborn, A.M. (2016) Molecular architecture of the retroviral capsid. *Trends Biochem. Sci.*, **41**, 410–420.
 56. Mendonca, L., Sun, D., Ning, J., Liu, J., Kotecha, A., Olek, M., Frosio, T., Fu, X., Himes, B.A., Kleinpeter, A.B. et al. (2021) CryoET structures of immature HIV Gag reveal six-helix bundle. *Commun. Biol.*, **4**, 481.
 57. Kong, J., Xu, B., Wei, W., Wang, X., Xie, W. and Yu, X.F. (2014) Characterization of the amino-terminal domain of Mx2/MxB-dependent interaction with the HIV-1 capsid. *Protein Cell*, **5**, 954–957.
 58. Buffone, C., Schulte, B., Opp, S. and Diaz-Griffero, F. (2015) Contribution of MxB oligomerization to HIV-1 capsid binding and restriction. *J. Virol.*, **89**, 3285–3294.
 59. Smaga, S.S., Xu, C., Summers, B.J., Digianantonio, K.M., Perilla, J.R. and Xiong, Y. (2019) MxB restricts HIV-1 by targeting the tri-hexamer interface of the viral capsid. *Structure*, **27**, 1234–1245.
 60. Diaz-Griffero, F., Vandegraaff, N., Li, Y., McGee-Estrada, K., Stremlau, M., Welikala, S., Si, Z., Engelman, A. and Sodroski, J. (2006) Requirements for capsid-binding and an effector function in TRIM5-mediated restriction of HIV-1. *Virology*, **351**, 404–419.
 61. Zhao, G., Ke, D., Vu, T., Ahn, J., Shah, V.B., Yang, R., Aiken, C., Charlton, L.M., Gronenborn, A.M. and Zhang, P. (2011) Rhesus TRIM5alpha disrupts the HIV-1 capsid at the inter-hexamer interfaces. *PLoS Pathog.*, **7**, e1002009.
 62. Yang, H., Ji, X., Zhao, G., Ning, J., Zhao, Q., Aiken, C., Gronenborn, A.M., Zhang, P. and Xiong, Y. (2012) Structural insight into HIV-1 capsid recognition by rhesus TRIM5alpha. *Proc. Natl. Acad. Sci. U.S.A.*, **109**, 18372–18377.
 63. Kovalsky, D.B. and Ivanov, D.N. (2014) Recognition of the HIV capsid by the TRIM5alpha restriction factor is mediated by a subset of pre-existing conformations of the TRIM5alpha SPRY domain. *Biochemistry*, **53**, 1466–1476.
 64. Li, Y.L., Chandrasekaran, V., Carter, S.D., Woodward, C.L., Christensen, D.E., Dryden, K.A., Pornillos, O., Yeager, M., Ganser-Pornillos, B.K., Jensen, G.J. et al. (2016) Primate TRIM5 proteins form hexagonal nets on HIV-1 capsids. *Elife*, **5**, e16269.
 65. Selyutina, A., Bulnes-Ramos, A. and Diaz-Griffero, F. (2018) Binding of host factors to stabilized HIV-1 capsid tubes. *Virology*, **523**, 1–5.
 66. Morger, D., Zosel, F., Buhlmann, M., Zuger, S., Mittelviehhaus, M., Schuler, B., Luban, J. and Grutter, M.G. (2018) The three-fold axis of the HIV-1 capsid lattice is the species-specific binding interface for TRIM5alpha. *J. Virol.*, **92**, e01541-17.
 67. Ganser-Pornillos, B.K. and Pornillos, O. (2019) Restriction of HIV-1 and other retroviruses by TRIM5. *Nat. Rev. Microbiol.*, **17**, 546–556.
 68. Price, A.J., Fletcher, A.J., Schaller, T., Elliott, T., Lee, K., KewalRamani, V.N., Chin, J.W., Towers, G.J. and James, L.C. (2012) CPSF6 defines a conserved capsid interface that modulates HIV-1 replication. *PLoS Pathog.*, **8**, e1002896.
 69. Matreyek, K.A., Yucel, S.S., Li, X. and Engelman, A. (2013) Nucleoporin NUP153 phenylalanine-glycine motifs engage a common binding pocket within the HIV-1 capsid protein to mediate lentiviral infectivity. *PLoS Pathog.*, **9**, e1003693.
 70. De Iaco, A., Santoni, F., Vannier, A., Guipponi, M., Antonarakis, S. and Luban, J. (2013) TNPO3 protects HIV-1 replication from CPSF6-mediated capsid stabilization in the host cell cytoplasm. *Retrovirology*, **10**, 20.
 71. Bhattacharya, A., Alam, S.L., Fricke, T., Zadrozny, K., Sedzicki, J., Taylor, A.B., Demeler, B., Pornillos, O., Ganser-Pornillos, B.K., Diaz-Griffero, F. et al. (2014) Structural basis of HIV-1 capsid recognition by PF74 and CPSF6. *Proc. Natl. Acad. Sci. U.S.A.*, **111**, 18625–18630.
 72. Yamashita, M. and Engelman, A.N. (2017) Capsid-dependent host factors in HIV-1 infection. *Trends Microbiol.*, **25**, 741–755.
 73. Rebenburg, S.V., Wei, G., Larue, R.C., Lindenberger, J., Francis, A.C., Annamalai, A.S., Morrison, J., Shkriabai, N., Huang, S.W., KewalRamani, V. et al. (2021) Sec24C is an HIV-1 host dependency factor crucial for virus replication. *Nat. Microbiol.*, **6**, 435–444.
 74. Price, A.J., Jacques, D.A., McEwan, W.A., Fletcher, A.J., Essig, S., Chin, J.W., Halambage, U.D., Aiken, C. and James, L.C. (2014) Host cofactors and pharmacologic ligands share an essential interface in HIV-1 capsid that is lost upon disassembly. *PLoS Pathog.*, **10**, e1004459.
 75. Dick, R.A., Zadrozny, K.K., Xu, C., Schur, F.K.M., Lyddon, T.D., Ricana, C.L., Wagner, J.M., Perilla, J.R., Ganser-Pornillos, B.K., Johnson, M.C. et al. (2018) Inositol phosphates are assembly co-factors for HIV-1. *Nature*, **560**, 509–512.
 76. Mallery, D.L., Marquez, C.L., McEwan, W.A., Dickson, C.F., Jacques, D.A., Anandapadamanam, M., Bichel, K., Towers, G.J., Saiardi, A., Bocking, T. et al. (2018) IP6 is an HIV pocket factor that prevents capsid collapse and promotes DNA synthesis. *Elife*, **7**, e35335.
 77. Jennings, J., Shi, J., Varadarajan, J., Jamieson, P.J. and Aiken, C. (2020) The host cell metabolite inositol hexakisphosphate promotes efficient endogenous HIV-1 reverse transcription by stabilizing the viral capsid. *mBio*, **11**, e02820-20.
 78. Yu, A., Lee, E.M.Y., Jin, J. and Voth, G.A. (2020) Atomic-scale characterization of mature HIV-1 capsid stabilization by inositol hexakisphosphate (IP6). *Sci Adv*, **6**, eabc6465.
 79. Dostalkova, A., Kaufman, F., Krizova, I., Vokata, B., Ruml, T. and Rumlova, M. (2020) In vitro quantification of the effects of IP6 and other small polyanions on immature HIV-1 particle assembly and core stability. *J. Virol.*, **94**, e00991-20.
 80. Mallery, D.L., Kleinpeter, A.B., Renner, N., Faysal, K.M.R., Novikova, M., Kiss, L., Wilson, M.S.C., Ahsan, B., Ke, Z.,

- Briggs, J.A.G. *et al.* (2021) A stable immature lattice packages IP6 for HIV capsid maturation. *Sci. Adv.*, **7**, eabe4716.
81. Rankovic, S., Ramalho, R., Aiken, C. and Rousso, I. (2018) PF74 reinforces the HIV-1 capsid to impair reverse transcription-induced uncoating. *J Virol*, **92**, e00845-18.
 82. Singh, K., Gallazzi, F., Hill, K.J., Burke, D.H., Lange, M.J., Quinn, T.P., Neogi, U. and Sonnerborg, A. (2019) GS-CA compounds: first-in-class HIV-1 capsid inhibitors covering multiple grounds. *Front Microbiol*, **10**, 1227.
 83. Zhou, J., Price, A.J., Halambage, U.D., James, L.C. and Aiken, C. (2015) HIV-1 resistance to the capsid-targeting inhibitor PF74 results in altered dependence on host factors required for virus nuclear entry. *J. Virol.*, **89**, 9068–9079.
 84. Carnes, S.K., Sheehan, J.H. and Aiken, C. (2018) Inhibitors of the HIV-1 capsid, a target of opportunity. *Curr. Opin. HIV AIDS*, **13**, 359–365.
 85. Cosnefroy, O., Murray, P.J. and Bishop, K.N. (2016) HIV-1 capsid uncoating initiates after the first strand transfer of reverse transcription. *Retrovirology*, **13**, 58.
 86. Rankovic, S., Varadarajan, J., Ramalho, R., Aiken, C. and Rousso, I. (2017) Reverse transcription mechanically initiates HIV-1 capsid disassembly. *J Virol*, **91**, 12. e00289-17.
 87. Rankovic, S., Deshpande, A., Harel, S., Aiken, C. and Rousso, I. (2021) HIV-1 uncoating occurs via a series of rapid biomechanical changes in the core related to individual stages of reverse transcription. *J. Virol.*, **95**, 10. e00166-21.
 88. Francis, A.C. and Melikyan, G.B. (2018) Single HIV-1 imaging reveals progression of infection through CA-dependent steps of docking at the nuclear pore, uncoating, and nuclear transport. *Cell Host Microbe*, **23**, 536–548.
 89. Alam, K.K., Chang, J.L., Lange, M.J., Nguyen, P.D.M., Sawyer, A.W. and Burke, D.H. (2018) Poly-target selection identifies broad-spectrum RNA aptamers. *Mol. Ther. Nucleic Acids*, **13**, 605–619.
 90. Lange, M.J., Nguyen, P.D.M., Callaway, M.K., Johnson, M.C. and Burke, D.H. (2017) RNA-protein interactions govern antiviral specificity and encapsidation of broad spectrum anti-HIV reverse transcriptase aptamers. *Nucleic Acids Res*, **45**, 6087–6097.
 91. Chen, L., Rashid, F., Shah, A., Awan, H.M., Wu, M., Liu, A., Wang, J., Zhu, T., Luo, Z. and Shan, G. (2015) The isolation of an RNA aptamer targeting to p53 protein with single amino acid mutation. *Proc. Natl. Acad. Sci. U.S.A.*, **112**, 10002–10007.
 92. Hermann, T. and Patel, D.J. (2000) Adaptive recognition by nucleic acid aptamers. *Science*, **287**, 820–825.
 93. Zichel, R., Chearwae, W., Pandey, G.S., Golding, B. and Sauna, Z.E. (2012) Aptamers as a sensitive tool to detect subtle modifications in therapeutic proteins. *PLoS One*, **7**, e31948.
 94. Thirunavukarasu, D. and Shi, H. (2015) An RNA aptamer specific to Hsp70-ATP conformation inhibits its ATPase activity independent of Hsp40. *Nucleic Acid Ther.*, **25**, 103–112.
 95. Moore, M.D., Bobay, B.G., Mertens, B. and Jaykus, L.A. (2016) Human norovirus aptamer exhibits high degree of target conformation-dependent binding similar to that of receptors and discriminates particle functionality. *mSphere*, **1**, e00298-16.
 96. Khsai, A.W., Wisler, J.W., Lee, J., Ahn, S., Cahill Iii, T.J., Dennison, S.M., Staus, D.P., Thomsen, A.R., Anastasi, K.M., Pani, B. *et al.* (2016) Conformationally selective RNA aptamers allosterically modulate the beta2-adrenoceptor. *Nat. Chem. Biol.*, **12**, 709–716.
 97. Weber, A.M., Kaiser, J., Ziegler, T., Pilsl, S., Renzl, C., Sixt, L., Pietruschka, G., Moniot, S., Kakoti, A., Juraschitz, M. *et al.* (2019) A blue light receptor that mediates RNA binding and translational regulation. *Nat. Chem. Biol.*, **15**, 1085–1092.
 98. Kim, S.J., Kim, M.Y., Lee, J.H., You, J.C. and Jeong, S. (2002) Selection and stabilization of the RNA aptamers against the human immunodeficiency virus type-1 nucleocapsid protein. *Biochem. Biophys. Res. Commun.*, **291**, 925–931.
 99. Ramalingam, D., Duclair, S., Datta, S.A., Ellington, A., Rein, A. and Prasad, V.R. (2011) RNA aptamers directed to human immunodeficiency virus type 1 Gag polypeptide bind to the matrix and nucleocapsid domains and inhibit virus production. *J Virol*, **85**, 305–314.
 100. Lochrie, M.A., Waugh, S., Pratt, D.G. Jr., Clever, J., Parslow, T.G. and Polisky, B. (1997) In vitro selection of RNAs that bind to the human immunodeficiency virus type-1 gag polypeptide. *Nucleic Acids Res.*, **25**, 2902–2910.
 101. Rose, K.M., Ferreira-Bravo, Alves, Li, I., Craigie, M., Ditzler, R., Holliger, M.A. and DeStefano, J.J. (2019) Selection of 2'-deoxy-2'-fluoroarabino nucleic acid (FANA) aptamers that bind HIV-1 integrase with picomolar affinity. *ACS Chem Biol*, **14**, 2166–2175.
 102. Li, N., Wang, Y., Pothukuchy, A., Syrett, A., Husain, N., Gopalakrishna, S., Kosaraju, P. and Ellington, A.D. (2008) Aptamers that recognize drug-resistant HIV-1 reverse transcriptase. *Nucleic Acids Res.*, **36**, 6739–6751.
 103. Lai, Y.T. and DeStefano, J.J. (2012) DNA aptamers to human immunodeficiency virus reverse transcriptase selected by a primer-free SELEX method: characterization and comparison with other aptamers. *Nucleic Acid Ther.*, **22**, 162–176.
 104. Tuerk, C., MacDougall, S. and Gold, L. (1992) RNA pseudoknots that inhibit human immunodeficiency virus type 1 reverse transcriptase. *Proc. Natl. Acad. Sci. U.S.A.*, **89**, 6988–6992.
 105. Burke, D.H., Scates, L., Andrews, K. and Gold, L. (1996) Bent pseudoknots and novel RNA inhibitors of type 1 human immunodeficiency virus (HIV-1) reverse transcriptase. *J. Mol. Biol.*, **264**, 650–666.
 106. Konopka, K., Lee, N.S., Rossi, J. and Duzgunes, N. (2000) Rev-binding aptamer and CMV promoter act as decoys to inhibit HIV replication. *Gene*, **255**, 235–244.
 107. Yamamoto, R., Katahira, M., Nishikawa, S., Baba, T., Taira, K. and Kumar, P.K. (2000) A novel RNA motif that binds efficiently and specifically to the Tat protein of HIV and inhibits the trans-activation by Tat of transcription in vitro and in vivo. *Genes Cells*, **5**, 371–388.
 108. Sayer, N., Ibrahim, J., Turner, K., Tahiri-Alaoui, A. and James, W. (2002) Structural characterization of a 2'-F-RNA aptamer that binds a HIV-1 SU glycoprotein, gp120. *Biochem. Biophys. Res. Commun.*, **293**, 924–931.
 109. Lange, M.J., Sharma, T.K., Whatley, A.S., Landon, L.A., Tempesta, M.A., Johnson, M.C. and Burke, D.H. (2012) Robust suppression of HIV replication by intracellularly expressed reverse transcriptase aptamers is independent of ribozyme processing. *Mol. Ther.*, **20**, 2304–2314.
 110. Rosa, A., Chande, A., Ziglio, S., De Sanctis, V., Bertorelli, R., Goh, S.L., McCauley, S.M., Nowosielska, A., Antonarakis, S.E., Luban, J. *et al.* (2015) HIV-1 Nef promotes infection by excluding SERINC5 from virion incorporation. *Nature*, **526**, 212–217.
 111. Yoo, S., Myszka, D.G., Yeh, C., McMurray, M., Hill, C.P. and Sundquist, W.I. (1997) Molecular recognition in the HIV-1 capsid/cyclophilin A complex. *J. Mol. Biol.*, **269**, 780–795.
 112. Wang, L., Casey, M.C., Vernekar, S.K.V., Sahani, R.L., Kirby, K.A., Du, H., Zhang, H., Tedbury, P.R., Xie, J., Sarafianos, S.G. *et al.* (2021) Novel PF74-like small molecules targeting the HIV-1 capsid protein: balance of potency and metabolic stability. *Acta Pharm. Sin. B*, **11**, 810–822.
 113. Wang, L., Casey, M.C., Vernekar, S.K.V., Sahani, R.L., Kankanala, J., Kirby, K.A., Du, H., Hachiya, A., Zhang, H., Tedbury, P.R. *et al.* (2020) Novel HIV-1 capsid-targeting small molecules of the PF74 binding site. *Eur. J. Med. Chem.*, **204**, 112626.
 114. Sousa, R. and Padilla, R. (1995) A mutant T7 RNA polymerase as a DNA polymerase. *EMBO J*, **14**, 4609–4621.
 115. McEntee, K., Weinstock, G.M. and Lehman, I.R. (1980) recA protein-catalyzed strand assimilation: stimulation by Escherichia coli single-stranded DNA-binding protein. *Proc. Natl. Acad. Sci. U.S.A.*, **77**, 857–861.
 116. Porciani, D., Cardwell, L.N., Tawiah, K.D., Alam, K.K., Lange, M.J., Daniels, M.A. and Burke, D.H. (2018) Modular cell-internalizing aptamer nanostructure enables targeted delivery of large functional RNAs in cancer cell lines. *Nat. Commun.*, **9**, 2283.
 117. Zadeh, J.N., Steenberg, C.D., Bois, J.S., Wolfe, B.R., Pierce, M.B., Khan, A.R., Dirks, R.M. and Pierce, N.A. (2011) NUPACK: analysis and design of nucleic acid systems. *J. Comput. Chem.*, **32**, 170–173.
 118. Porciani, D., Signore, G., Marchetti, L., Mereghetti, P., Nifosi, R. and Beltram, F. (2014) Two interconvertible folds modulate the activity of a DNA aptamer against transferrin receptor. *Mol. Ther. Nucleic Acids*, **3**, e144.